Title
The Abca7V1613M variant reduces Aβ generation, plaque load, and neuronal damage

Journal
Alzheimer's & Dementia, 20(7)

ISSN
1552-5260

Authors
Butler, Claire A
Arvilla, Adrian Mendoza
Milinkeviciute, Giedre
et al.

Publication Date
2024-07-01

DOI
10.1002/alz.13783

Peer reviewed

Received: 9 October 2023 | Revised: 21 December 2023 | Accepted: 23 December 2023

DOI: 10.1002/alz.13783

Alzheimer's & Dementia®
THE JOURNAL OF THE ALZHEIMER'S ASSOCIATION

RESEARCH ARTICLE

The *Abca7*^{V1613M} variant reduces Aβ generation, plaque load, and neuronal damage

Claire A. Butler[1,2] | **Adrian Mendoza Arvilla**[2] | **Giedre Milinkeviciute**[2] | **Celia Da Cunha**[2] | **Shimako Kawauchi**[2,3] | **Narges Rezaie**[4,5] | **Heidi Y. Liang**[4,5] | **Dominic Javonillo**[1] | **Annie Thach**[2] | **Shuling Wang**[3] | **Sherilyn Collins**[3] | **Amber Walker**[3] | **Kai-Xuan Shi**[3] | **Jonathan Neumann**[3] | **Angela Gomez-Arboledas**[2] | **Caden M. Henningfield**[1] | **Lindsay A. Hohsfield**[1] | **Mark Mapstone**[2,6] | **Andrea J. Tenner**[1,7,8] | **Frank M. LaFerla**[1,2] | **Ali Mortazavi**[4,5] | **Grant R. MacGregor**[3,4] | **Kim N. Green**[1,2]

[1]Department of Neurobiology and Behavior, University of California, Irvine, California, USA

[2]Institute for Memory Impairments and Neurological Disorders, University of California, Irvine, California, USA

[3]Transgenic Mouse Facility, ULAR, Office of Research, University of California, Irvine, California, USA

[4]Department of Developmental and Cell Biology, University of California, Irvine, California, USA

[5]Center for Complex Biological Systems, University of California, Irvine, California, USA

[6]Department of Neurology, University of California, Irvine, California, USA

[7]Department of Molecular Biology & Biochemistry, University of California, Irvine, California, USA

[8]Department of Pathology and Laboratory Medicine, University of California, Irvine, California, USA

Correspondence
Kim N. Green, 3208 Biological Sciences III, University of California, Irvine, Irvine, CA 92697-4545, USA.
Email: kngreen@uci.edu

Grant R. MacGregor, D.Phil., 4213 McGaugh Hall, University of California, Irvine, Irvine, CA 92697-4545, USA.
Email: gmacg@uci.edu

Funding information
National Institute on Aging, Grant/Award Number: U54 AG054349; Cancer Center Support, Grant/Award Number: CA-62203; Center for Complex Biological Systems Support, Grant/Award Number: GM-076516

Abstract

BACKGROUND: Variants in *ABCA7*, a member of the ABC transporter superfamily, have been associated with increased risk for developing late onset Alzheimer's disease (LOAD).

METHODS: CRISPR-Cas9 was used to generate an *Abca7*^{V1613M} variant in mice, modeling the homologous human *ABCA7*^{V1599M} variant, and extensive characterization was performed.

RESULTS: *Abca7*^{V1613M} microglia show differential gene expression profiles upon lipopolysaccharide challenge and increased phagocytic capacity. Homozygous *Abca7*^{V1613M} mice display elevated circulating cholesterol and altered brain lipid composition. When crossed with 5xFAD mice, homozygous *Abca7*^{V1613M} mice display fewer Thioflavin S-positive plaques, decreased amyloid beta (Aβ) peptides, and altered amyloid precursor protein processing and trafficking. They also exhibit reduced Aβ-associated inflammation, gliosis, and neuronal damage.

DISCUSSION: Overall, homozygosity for the *Abca7*^{V1613M} variant influences phagocytosis, response to inflammation, lipid metabolism, Aβ pathology, and neuronal damage in mice. This variant may confer a gain of function and offer a protective effect against Alzheimer's disease-related pathology.

KEYWORDS
ABCA7, Alzheimer's disease, Aβ, lipids, neuroinflammation

Highlights

- *ABCA7* recognized as a top 10 risk gene for developing Alzheimer's disease.
- Loss of function mutations result in increased risk for LOAD.
- V1613M variant reduces amyloid beta plaque burden in 5xFAD mice.
- V1613M variant modulates APP processing and trafficking in 5xFAD mice.
- V1613M variant reduces amyloid beta-associated damage in 5xFAD mice.

1 | BACKGROUND

Alzheimer's disease (AD) is a progressive neurodegenerative disease characterized by the presence of extracellular amyloid beta (Aβ) plaques and intracellular neurofibrillary tau tangles.[1] Causative mutations in genes related to amyloid precursor protein (APP) processing have been identified for autosomal dominant AD. In contrast, the disease etiology for sporadic or late-onset AD (LOAD) remains unclear. To better understand this, genome-wide association studies (GWAS) have identified genetic variations associated with risk of developing LOAD,[2–4] including variants in *ABCA7*.[2,3,5]

ABCA7 encodes ATP-binding cassette, subfamily A, member 7 (ABCA7), a multidomain transmembrane protein member of the conserved superfamily of ATP-binding cassette (ABC) transporters that transfer various molecules across membranes in an ATP-dependent manner.[6] ABCA7 mediates efflux of phospholipids and to a much lesser extent cholesterol across the plasma membrane.[7–9,10] In *Abca7* knockout (KO) mice, cholesterol metabolism, characterized by reduced plasma high-density lipoprotein (HDL) and cholesterol levels, brain lipid profiles, and lipid rafts in antigen-presenting cells, are all disrupted compared to wildtype (WT) littermates.[11–14] ABCA7 deficiency also reduced phagocytosis of apoptotic cells, Aβ oligomers, and diminished proinflammatory response in macrophages.[15–17] In transgenic AD mouse models, complete or haploinsufficiency of *Abca7* results in increased Aβ accumulation in the brain and reduced uptake of Aβ in macrophages and microglia.[16,18] ABCA7 loss of function also increases Aβ via altered APP processing.[19]

Consistent with these findings, rare premature termination codon and/or loss of function mutations in *ABCA7* have been associated with increased risk of AD and are enriched in AD patients,[20] whereas a low-frequency coding variant (p.G215S) has been identified as potentially protective against AD.[21] Additional study is needed to understand the biological implications of specific *ABCA7* polymorphisms in AD.

Despite being a major risk factor for AD, there is limited knowledge on the role of ABCA7 in the development and progression of AD, particularly regarding the impact of specific variants on AD risk and disease pathology. One specific *ABCA7* single nucleotide polymorphism (SNP), *rs117187003*, produces the rare V1599M variant in humans. Several exome sequencing studies predicted this variant, which is located in a region of ABCA7 that is conserved between humans and mouse, as being deleterious and potentially damaging.[4,21] To test the hypothesis that this variant is potentially damaging we used CRISPR-CAS9 to introduce the corresponding coding variant (V1613M) in the mouse genome, which we refer to as *Abca7*^{V1613M} hereafter. Homozygous *Abca7*^{V1613M} microglia exhibit a more inflammatory response to acute lipopolysaccharide (LPS) stimulation and have increased phagocytic capacity for Aβ1-42 and beads. To examine the impact of this genetic variation on AD pathology, we analyzed homozygous *Abca7*^{V1613M} mice that were hemizygous for the 5xFAD transgene array. 5xFAD/*Abca7*^{V1613M} mice have altered brain and plasma lipids, reduced Aβ plaques, neuroinflammation, dystrophic neurites, and neurofilament light chain (NfL) levels. Finally, we used both in vivo and in vitro approaches to show that the *Abca7*^{V1613M} variant induces alterations in APP processing and trafficking. These results suggest that the effects of the *Abca7*^{V1613M} variant are consistent with a gain of function, rather than a loss of function, and may offer protection against the development of LOAD.

2 | METHODS

2.1 | Animals

All experiments involving mice were approved by the UC Irvine (UCI) Institutional Animal Care and Use Committee (IACUC) and were conducted in compliance with all relevant ethical regulations for animal testing and research. All experiments involving mice comply with

the Animal Research: Reporting of in Vivo Experiments (ARRIVE-10) guidelines.

2.2 | Mouse generation and breeding

CRISPR/Cas9 was used to generate a V1613M missense variant allele of *Abca7*. This variant models a SNP (rs117187003) in human *ABCA7* that encodes a missense variant (V1599M). Alt-R Crispr RNA (TMF1268—cttggtggcagtgtgcatag) and tracrRNA plus CAS9 protein (HiFi Cas9 nuclease V3, Integrated DNA Technologies [IDT), Coralville, IA) as a ribonucleoprotein (RNP) were electroporated into C57BL/6J zygotes (Jackson Lab Stock # 000664) along with a ssODN sequence (TMF1276—sequence available upon request) to introduce the V1613M missense variant. G0 founder animals containing the desired DNA sequence changes were backcrossed with C57BL/6J mice, and N1 *Abca7*^{V1613M} heterozygous mice were sequenced to determine the variant allele. N1 *Abca7*^{V1613M} heterozygous mice were again backcrossed with C57BL/6J mice to produce N2F1 *Abca7*^{V1613M} heterozygotes, which were subsequently crossed with 5xFAD hemizygous congenic B6J (B6.CgTg(APPSwFlLon,PSEN1*M146L*L286V)6799Vas/Mmjax, Jackson Lab Stock # 34848, MMRRC) mice to produce N3F1 animals that were heterozygous or wildtype for *Abca7*^{V1613M} and hemizygous or nontransgenic for 5xFAD. These N3F1 animals were used to produce N3Fx experimental and control animals by natural mating or in vitro fertilization procedures (Figure S1). After weaning, they were housed together by sex with littermates and aged until the harvest dates. All animals in this study were on a co-isogenic or congenic C57BL/6J strain background. All animals were bred by the Transgenic Mouse Facility at UCI. *Abca7*^{V1613M} mice (B6- *Abca7* ^{em1Aduci}/J) are available from The Jackson Laboratory (Bar Harbor, ME), stock number #035316.

2.3 | Genotyping

Oligonucleotides for polymerase chain reaction (PCR)-based genotyping were purchased from IDT. *Abca7*^{V1613M} genotyping was performed using a common primer set to amplify both *Abca7* wildtype allele and *Abca7*^{V1613M} allele (For 5′- TGGATACAGTGTAACTACTTGG –3′ and Rev 5′- ATAGGCTCTCTGCTGAAAG –3′). Two fluorophore labeled-hydrolysis probes which hybridized specific to mouse *Abca7* wildtype amplicon (5′- TGAACACCACTATGCACACTGCCA –3′+HEX) and *Abca7*^{V1613M} variant (5′- TGA ACATGACGATGCACACTGCCA –3′-FAM) were used to detect the allelic ratio in the amplicon. The relative fluorescence from each probe was quantified at the end point of PCR cycles to call the genotype using the allelic discrimination function in Bio-Rad CFX Maestro software (Bio-Rad, Hercules, CA). For 5xFAD genotyping, a hydrolysis probe which hybridizes to APP(Swe) mutation amplicon was used (For 5′-TGGGTTCAAACAAAGGTGCAA-3′ and Rev 5′-GATGACGATCACTGTCGCTATGAC-3′: APP(Swe) probe 5′-CATTGGACTCATGGTGGGCGGTG-3′) to detect transgenes. We used endogenous *ApoB* allele (For 5′-CACGTGGGCTCCAGCATT-3′ and Rev 5′-TCACCAGTCATTTCTGCCTTTG-3′: *ApoB* probe 5′-CCAATGGTCGGGCACTGCTCAA-3′) to normalize the cycle threshold values.

RESEARCH IN CONTEXT

1. **Systematic review**: The authors reviewed the literature using traditional (eg, PubMed) sources and meeting abstracts and presentations. While the role of *ABCA7*, and its variants, in Alzheimer's disease (AD) pathogenesis is not yet as widely studied as other aspects of AD biology, there have been several publications using *Abca7* knockout models which have highlighted a key role for ABCA7 in amyloid beta (Aβ) production and processing. These relevant works are appropriately cited.
2. **Interpretation**: Our findings show introduction of *Abca7*^{V1613M} variant modulates Aβ production, processing, and ultimately results in reduced Aβ plaque formation and the variant protects against Aβ-induced damage in a 5xFAD mouse model.
3. **Future directions**: This study highlights the effect of the *Abca7*^{V1613M} variant on Aβ pathology. Further work is required to understand the underlying molecular mechanisms of ABCA7 and variant function and whether promoting ABCA7 function may be beneficial to treatment of AD.

2.4 | Off-target analysis

Genomic DNA was extracted from mouse tail biopsies using DirectPCR Lysis Reagent (Viagen Biotech, Los Angeles, CA) and Proteinase K (Roche, Indianapolis, IN). Amplification was performed using a Bio-Rad CFX-96 instrument. For each amplicon, a single PCR product was confirmed by capillary electrophoresis (Fragment Analyzer, AATI / Agilent, Santa Clara, CA) then subjected to Sanger sequencing (Retrogen, San Diego, CA) and analyzed using SeqMan Pro 17.2 (DNASTAR, Madison, WI). Potential off-target sites are listed in Table S1 while primers for PCR amplification and sequencing of potential off-target sites are listed in Table S2.

2.5 | Bulk RNA-sequencing

Frozen hippocampi were pulverized, and total RNA was extracted according to manufacturer's instructions using RNAeasy Plus mini kit (Qiagen, 74134). The RNA integrity number (RIN) was measured, and samples with RIN $\geq$ 7.0 were kept for library construction. cDNA synthesis, amplification, library construction, and sequencing were performed by Novogene (Sacramento, CA) using Illumina NovaSeq and

HiSeq platforms with paired-end 150 bp (PE 150) sequencing strategy. Fastqs were aligned to the mouse genome (mm10) and annotation was done using GENCODE v21. Pair-end RNA-seq reads were mapped with STAR (2.5.1b-static) and RSEM (1.2.22) was used for quantification of gene expression.

2.5.1 | Differential gene expression analysis

Differential gene expression analysis was performed using edgeR per timepoint and genotype or treatment on polyA genes. Top significant genes are displayed as a volcano plot constructed using GLimma, ggplot2, and EnhancedVolcano (false discovery rate [FDR] < 0.05, LogFC > 1). Based on the differentially expressed gene (DEG) comparisons, gene transcripts per million (TPMs) of interest were plotted as a heatmap or graphically using Prism (GraphPad, Boston, MA).

2.5.2 | Weighted correlation gene network analysis

Weighted gene correlation network analysis (WGCNA) was performed using PyWGCNA[22] on the *Abca7*^{V1613M} dataset with matching controls at two different timepoints (4 months and 12 months old) in the hippocampus for both sexes, using genes with more than 1 TPM. One sample was removed based on hierarchical clustering at the sample level. Based on our datasets, we used power 19 as a soft threshold. PyWGCNA were also applied on the LPS dataset (Figure 1) at all three timepoints (0 hours, 6 and 24 hours) for both treatment groups using genes with more than 1 TPM. The other parameters were the same for both including min. module size = 50 and MEDissThres = 0.2. Significant modules were identified by calculating the correlation with the traits, then plotting the behavior per sample of the genes in the inflammatory module by doing a GO term analysis using PyWGCNA.

2.6 | LPS treatment

Eight-month-old WT and homozygous *Abca7*^{V1613M} mice of both sexes were injected intraperitoneally with either 0.3 mg/kg LPS or 1× phosphate-buffered saline (PBS). At 6 or 24 hours post administration, mice were euthanized via CO_2 inhalation and transcardially perfused with ice-cold 1× PBS. Brains were removed and hemispheres separated along the midline. Brain halves were flash frozen for RNA-sequencing analysis.

2.7 | Generation of mouse mixed primary microglia-astrocyte cultures

Primary mixed microglia-astrocyte cultures were generated as described.[23] Whole brains were extracted from neonatal 3- to 5-day-old mice and cortical tissue was cut into small pieces before digestion with trypsin. Trypsin was quenched using glia media (DMEM supplemented with 10% performance + heat inactivated serum (10082147; Thermo Fisher Scientific) and 1% penicillin/streptomycin (P4333-100ML; Sigma-Aldrich) and tissue was dissociated by pipetting up and down 20 times with a 1000-μL tip. Following digestion, the tissue was dissociated and homogenized through pipetting and then centrifuged at 150 × *g* for 7 minutes with slow start-stop at room temperature. Cells were resuspended in fresh glia media and filtered using 100-μm (352360; Falcon), followed by 40-μm strainers (352340; Falcon). Finally, the cells were reconstituted with 10 mL of glia media and placed in T-75 cm^2 flasks. Flasks were precoated with 0.002% poly-lysine (P4707-50ML; Sigma-Aldrich) for at least 30 minutes, at room temperature. After 24 hours, 20 mL of fresh media was added to the cell cultures. After 7 to 14 days in vitro, mixed microglia-astrocyte cultures were used for experiments.

2.8 | Phagocytosis assays

Primary microglia were removed from mixed microglia-astrocyte culture by gentle shaking as described.[23] To investigate the ability of cells to engage in general phagocytosis, 0.005% w/v 5-μm carboxylated beads (CFP-5070-2; Spherotech) were incubated for 2 hours with 50,000 primary microglia (seeded in 2:1 fresh:conditioned DMEM in 24-well plates in triplicate 24 hours before adding cargo). For Alexa Fluor 647-labelled Aβ1-42 (AS-64161; AnaSpec) a final concentration of 2 μM was added for 1 hour to a total of 20,000 primary microglia (seeded in 2:1 fresh:conditioned DMEM in 96-well plates in triplicate 24 hours before adding cargo). For both experiments, microglia were pretreated +/- 10 μM cytochalasin D (CytD) for 1 hour as a negative control for phagocytic uptake. After incubation, cells were washed twice with PBS to remove non-phagocytosed cargo and then harvested using trypsin, pelleted, and finally resuspended in PBS for flow cytometry (NovoCyte, Agilent, Santa Clara, CA).

2.9 | Flow cytometry

For flow cytometry, ACEA Quanteon (NovoCyte) analyzer was used. At least 5000 events were analyzed for each treatment replicate. Fc blocking antibodies were not used. Forward and side scatter was used to distinguish cells from unphagocytosed targets, that is, beads and Aβ, by gating on cells in the forward and side scatter plots. Within this scatter gate, a fluorescence gate was set to identify cells that were over a threshold of fluorescence. For phagocytic targets, this fluorescence gate was set so that for cells incubated in the absence of any fluorescent targets (ie, absence of fluorescent beads or Aβ), 99% of the cells were below this gated fluorescence and 1% were above this gate. For cells incubated in the presence of fluorescent targets, the percentage of cells with fluorescence greater than the gated fluorescence was used as the measure of mean fluorescence intensity of cells that had phagocytosed the targets. For detection of 5-μm sky blue fluorescent beads and Aβ– Alexa Fluor 647, a 640-nm excitation laser and allophycocyanin (APC) detector were used.

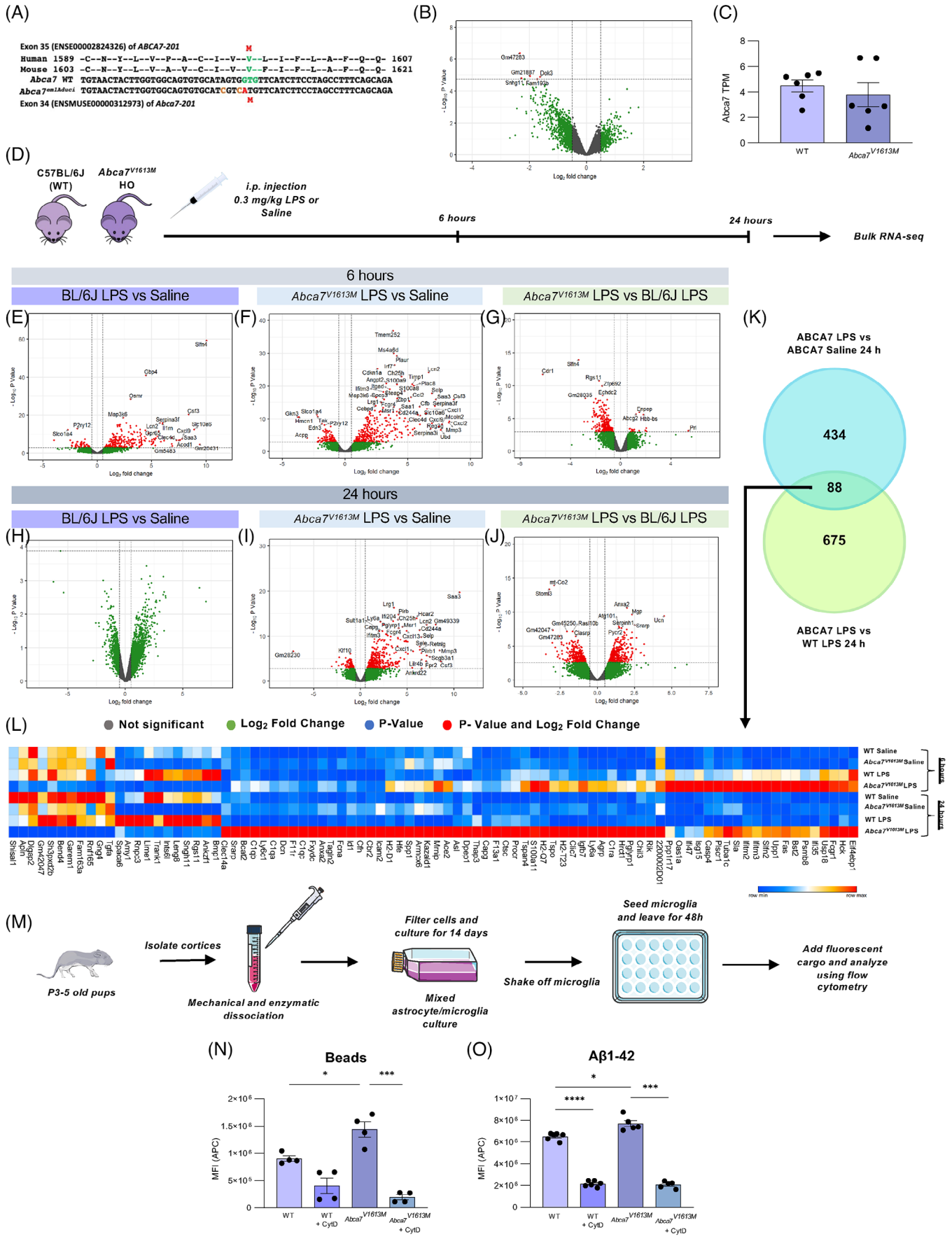
(A)
Exon 35 (ENSE00002824326) of ABCA7-201
Human 1589 -C--N--Y--L--V--P--A--C--I--V--V--L--I--F--L--A--F--Q--Q- 1607
Mouse 1603 -C--N--Y--L--V--A--V--C--I--V--V--F--I--F--L--A--F--Q--Q- 1621
Abca7 WT TGTAACTACTTGGTGGCAGTGTGCATAGTGGTGTTCATCTTCCTAGCCTTTCAGCAGA
Abca7 TGTAACTACTTGGTGGCAGTGTGCATCGTCATGTTCATCTTCCTAGCCTTTCAGCAGA
Exon 34 (ENSMUSE00000312973) of Abca7-201
(B)
(C)
Abca7 TPM
WT
Abca7V1613M
(D)
C57BL/6J (WT)
Abca7V1613M HO
i.p. injection 0.3 mg/kg LPS or Saline
6 hours
24 hours
Bulk RNA-seq
6 hours
BL/6J LPS vs Saline
Abca7V1613M LPS vs Saline
Abca7V1613M LPS vs BL/6J LPS
(E)
(F)
(G)
24 hours
BL/6J LPS vs Saline
Abca7V1613M LPS vs Saline
Abca7V1613M LPS vs BL/6J LPS
(H)
(I)
(J)
(K)
ABCA7 LPS vs ABCA7 Saline 24 h
434
88
675
ABCA7 LPS vs WT LPS 24 h
(L)
Not significant
Log2 Fold Change
P-Value
P- Value and Log2 Fold Change
WT Saline
Abca7V1613M Saline
WT LPS
Abca7V1613M LPS
6 hours
24 hours
row min
row max
(M)
P3-5 old pups
Isolate cortices
Mechanical and enzymatic dissociation
Filter cells and culture for 14 days
Mixed astrocyte/microglia culture
Shake off microglia
Seed microglia and leave for 48h
Add fluorescent cargo and analyze using flow cytometry
(N)
Beads
MFI (APC)
WT
WT + CytD
Abca7V1613M
Abca7V1613M + CytD
(O)
Aβ1-42
MFI (APC)
WT
WT + CytD
Abca7V1613M
Abca7V1613M + CytD

2.10 | Lipid/cholesterol Piccolo analysis

Blood plasma was collected and analyzed using a Piccolo blood chemistry analyzer (Abaxis, Union City, CA) according to the manufacturer's instructions. Briefly, plasma was diluted 1:1 with ddH_20 and 100 μL was loaded onto the Piccolo lipid plus panel plate (#07P0212, Abaxis). For lipid analysis, total cholesterol (CHOL), HDL, non-HDL cholesterol (nHDLc), triglycerides, low-density lipoprotein (LDL), and very LDL (vLDL) were analyzed and plotted. Lipid and general chemistry controls (#07P0401, Abaxis) were used.

2.11 | Bulk lipidomics

Lipid analysis was conducted by UC Davis West Coast Metabolomics Center as described.[24] Briefly, 1 mL of ice-cold solvent mixture (N_2-purged 3:10 methanol:methyl-tertiary butyl ether) was added to 2 mg (dry weight) of pulverized cortical tissue, followed by lipophilic/hydrophilic phase separation. The upper organic phase was transferred into two separate tubes and was analyzed via a Charged Surface Hybrid column. The lower aqueous phase was transferred into two separate tubes and was analyzed by hydrophilic interaction liquid chromatography. The abundance of 552 lipids were quantified for the WT, 5xFAD hemizygous, *Abca7*^{V1613M} homozygous, and 5xFAD hemizygous/*Abca7*^{V1613M} homozygous (ie, 5xFAD/*Abca7*^{V1613M}) mice. Raw lipid abundances were log10 transformed and pareto scaled prior to analysis. Metaboanalyst 5.0 (http://Metaboanalyst.ca) was used for all lipidomic analyses. Analysis of variance (ANOVA) with Tukey's post hoc test was used to examine group differences in the lipidomic profiles. Differential abundance of the lipids was calculated using a fold change of >1.5 or an FDR *p*-value of <0.05 for significance.

2.12 | Histology

Mice were euthanized at 4 and 12 months old and brain hemispheres were drop-fixed in 4% paraformaldehyde (PFA) for immunohistochemical analysis. Fixed half brains were cryopreserved with 0.05% sodium azide and 30% sucrose and stored at 4°C before being sliced at 40 μm using a Leica SM2000R freezing microtome (between −2.78 mm posterior and −3.38 mm posterior to Bregma according to the Allen Mouse Brain Atlas, Reference Atlas version 1, 2008). Sliced brains were placed in 30% ethyl glycerol and 30% glycerol at −20°C for long-term storage. One representative brain slice from each mouse of the same experimental group (ie, same genotype, age, and sex) was stained. Free-floating sections were washed three times with 1× PBS (1 × 10 minutes and 2 × 5 minutes) and for Thioflavin S (ThioS) staining, incubated for 10 minutes in 0.5% ThioS (T1892; Sigma-Aldrich) diluted in 50% ethanol. Sections were washed 2 × 5 minutes each in 50% ethanol and 1 × 10 minutes in 1× PBS. For Amylo-Glo staining, after PBS washes, brain slices were washed in 70% ethanol for 5 minutes and rinsed in ddH_2O for 2 minutes before being immersed for 10 minutes in Amylo-Glo RTD Amyloid Plaque Staining Reagent (1:100; TR-200-AG; Biosensis, Temecula, CA) diluted in 0.9% saline solution. Afterwards, sections were washed in 0.9% saline solution for 5 minutes, then rinsed in deionized water for 15 seconds before proceeding with a standard indirect immunohistochemical protocol. After staining with ThioS or Amylo-Glo, sections were protected from light. Sections were immersed in blocking solution (5% normal goat serum with 0.2% Triton X-100 in 1× PBS) for 1 hour before overnight incubation at 4°C with primary antibodies diluted in normal blocking serum solution.

Brain sections were stained following a standard indirect technique as described[25–27] with the following primary antibodies against ionized calcium-binding adapter molecule 1 (IBA1; 1:2000; 019–19741; Wako or IBA1, 1:1000, 234 009, Synaptic systems), cluster

FIGURE 1 The *Abca7*^{V1613M} allele in mice models the human single nucleotide polymorphism rs117187003 (*ABCA7*^{V1599M}) and induces distinct responses to lipopolysaccharide (LPS) challenge and increased phagocytosis. (A) Human and mouse amino acid sequence alignment indicating position of valine (V) to methionine (M) missense variant in each species (in green/red). Two silent mutations (tan) were co-introduced into mouse *Abca7* to prevent recutting of the edited allele by CRISPR-Cas9. (B) Volcano plot of differentially expressed genes (DEGs) between C57BL6/J (wildtype [WT]) and *Abca7*^{V1613M} homozygous mice at 6 to 8 months of age. Only five DEGs were deemed significant (denoted by red dots). (C) Transcripts per million (TPMs) of *Abca7* in WT and *Abca7*^{V1613M} homozygotes (unpaired Student *t*-test). (D) Experimental paradigm used for the LPS experiment. I Volcano plot of DEGs between WT mice treated with 0.3 mg/kg LPS versus saline 6 hours postinjection. (F) Volcano plot of DEGs between *Abca7*^{V1613M} mice treated with 0.3 mg/kg LPS versus saline 6 hours postinjection. (G) Volcano plot of DEGs between *Abca7*^{V1613M} and WT B6/J mice treated with 0.3 mg/kg LPS 6 hours postinjection. (H) Volcano plot of DEGs between *Abca7*^{V1613M} mice treated with 0.3 mg/kg LPS versus saline 24 hours postinjection. (I) Volcano plot of DEGs between *Abca7*^{V1613M} mice treated with 0.3 mg/kg LPS versus saline 24 hours postinjection. (J) Volcano plot of DEGs between *Abca7*^{V1613M} and WT mice treated with 0.3 mg/kg LPS 24 hours post injection. (K) Venn diagram highlighting the 88 overlapping genes between *Abca7*^{V1613M} LPS versus *Abca7*^{V1613M} saline and *Abca7*^{V1613M} LPS versus WT LPS DEGs at 24 hours. (L) Heatmap of 88 overlapping genes between *Abca7*^{V1613M} LPS versus saline mice and *Abca7*^{V1613M} and WT LPS treated mice 24 hours postinjection highlighting increased expression of inflammatory genes in *Abca7*^{V1613M} mice compared to WT mice at both 6 and 24 hours postinjection. $N = 3$ to 4 mice per genotype/treatment/timepoint. Mice from each genotype/treatment/timepoint were pooled and the mean TPM value was plotted as the heatmap. A $\log_2$ fold change of 0.5 was used for all volcano plots; however, the $-\log_{10}$ *p*-value changed according to different comparisons analyzed. (M) Schematic of primary microglial extraction from neonatal pups. (N,O) Uptake assays of primary microglia extracted from WT and *Abca7*^{V1613M} mice for (N) carboxylated beads, $N = 4$ independent experiments, and (O) Aβ 1-42 peptide, $N = 5$ independent experiments; one-way analysis of variance was used to examine group differences. MFI (APC) indicates the mean fluorescence intensity of allophycocyanin (APC) fluorophore inside microglia; 10 μM cytochalasin D was used as an inhibitor for phagocytosis. Data are represented as mean ± SEM. $^{*}p \leq 0.05$, $^{***}p \leq 0.001$, $^{****}p \leq 0.0001$.

of differentiation 68 (CD68; 1:500; AB125212; ABCAM), Aβ1-16 (6E10; 1:2000; 8030001; BioLegend), glial fibrillary acidic protein (GFAP; 1:1000; AB134436; Abcam), S100 calcium binding protein β (S100β; 1:200; AB41548; Abcam), lysosome-associated membrane protein 1 (LAMP1; 1:200; AB25245, Abcam), BASSOON (1:250, 75-491, NeuroMab), HOMER1 (1:250; 160003, SYSY), OC (1:1000; AB2286; Sigma-Aldrich), and CD11c (1:100, 14-0114-82, Invitrogen). Brain sections were mounted on poly-lysine microscope slides using polyvinylpyrrolidone (AC227541000; Thermo Fisher Scientific) then cover slipped (48393-106, Avantor) using Fluoromount-G (0100-01, Southern Biotech).

Images of whole hemispheres were acquired with a Zeiss Axio Scan Z1 Slidescanner (Carl Zeiss), using a 10 × 0.45 NA Plan-Apo objective. High-resolution fluorescence images were obtained using a Leica TCS SPE-II confocal microscope and LAS-X software. For confocal imaging, one field of view per brain region was acquired per mouse.

For super-resolution imaging of synaptic puncta, images of the visual cortex, subiculum, and CA1 regions were acquired using Super–Resolution Lattice Structured Illumination Microscopy (Lattice-SIM) with an Elyra 7 microscope system (Carl Zeiss, White Plains, NY). Samples were imaged using a 63 × 1.4 NA Plan-Apo objective lens and Immersol 518 F (23°C) immersion oil. Images were collected as z-stacks (110 nm step interval, within a depth of 3 to 8 μm, covering an area of 64 × 64 μm) and for each focal plane, nine phase images were acquired. Images were then processed using ZEN SIM_2 with ZEN software (black edition, Zeiss). Two images per brain region/mouse/genotype/age/sex were acquired.

2.13 | Imaris quantitative analysis

Image analysis was performed and quantified using Imaris 9.7 Software (Bitplane, South Windsor, CT). Confocal images of Aβ plaques, LAMP1 halos, microglia, and astrocytes were quantified using the spots module. Similarly, volumetric measurements (ie, ThioS+ plaque volume, IBA1+ microglia volume, etc.) were acquired utilizing the surfaces module. Quantitative comparisons between experimental groups were carried out in sections stained simultaneously. For synaptic quantification, the total number of BASSOON or HOMER1 puncta was quantified using the spots function on Imaris. Results were normalized to the total volume of each image, to correct for any difference in the depth of imaging.

2.14 | Quantification of soluble and insoluble fraction Aβ and NfL

Preparation of samples and quantification of Aβ was performed as described.[25–27] Microdissected hippocampal and cortical regions of each mouse were flash-frozen and processed for biochemical analysis. Samples were pulverized using a Bessman Tissue Pulverizer. Pulverized hippocampal tissue was homogenized in 150 μL of Tissue Protein Extraction Reagent (TPER; Life Technologies, Carlsbad, CA), while cortical tissue was homogenized in 1000 μL/150 mg of TPER. This composition of TPER includes 25 mM bicine and 150 mM sodium chloride (pH 7.6) to efficiently solubilize proteins within brain tissue following homogenization. Together with protease (11836170001, Roche) and phosphatase inhibitors (78426, Thermo Fisher Scientific), the homogenized samples were centrifuged at 100,000 × *g* for 1 h at 4°C to generate TPER-soluble fractions. For formic acid-fractions, TPER-insoluble pellets were homogenized in 70% formic acid. Afterwards, samples were again centrifuged at 100,000 × *g* for 1 hour at 4°C. Protein in the insoluble fraction of microdissected hippocampal and cortical tissue was normalized to its respective brain region weight, while protein in soluble fractions was normalized to the protein concentration determined via Bradford Protein Assay. Formic acid neutralization buffer (1 M Tris base, 0.5 M Na_2HPO_4, 10% NaN_3) was used to adjust pH prior to running Meso Scale Discovery (MSD) assays.

Human Aβ in soluble and insoluble fractions was measured using the V-PLEX Aβ Peptide Panel 1 (6E10) (K15200G-1; Meso Scale Discovery, Rockville, MD). Plasma NfL was measured using the R-Plex Human Neurofilament L Assay (K1517XR-2; Meso Scale Discovery). Mouse Aβ levels in N2a cell lines were measured using V-PLEX Aβ peptide Panel 1 (4G8) (K15199G-2; Meso Scale Discovery) and mouse plasma proinflammatory cytokines were measured using V-PLEX mouse proinflammatory cytokine Panel 1 (K15048D-1; Meso Scale Discovery)

2.15 | Western blotting

The cortical soluble protein fraction extracted for Aβ MSD assay was also used for western blotting. Protein concentrations were determined by the Pierce protein assay (22660; Thermo Fisher Scientific, Waltham, MA). Proteins were separated by sodium dodecyl sulfate-polyacrylamide gel electrophoresis (SDS-PAGE) through a 4% to 12% Bis/Tris gel (Life Technologies) for 2.5 hours at 80 V for APP blots and 1.5 hour at 100 V for all other blots. Proteins were transferred to 0.22 μM nitrocellulose membranes (926-31092, LI-COR, Lincoln, NE) and stained with REVERT 700 total protein stain (TPS; 926-11016, LI-COR) for 5 minutes at room temperature. After a brief rinse, the TPS was quantified using Image Studio software and an Odyssey CLx with TPS values used for subsequent normalization. Membranes were then blocked for 1 hour in Odyssey block solution (927-50000; LI-COR). Primary antibodies and dilutions used in this study include the following: 6E10 for full-length APP (1:1000, 803002, BioLegend), C-terminal (751-770) APP for C99 and C83 fragments (1:1000, 17161050UL, MilliporeSigma), BACE1 (1:1000, AB2077, ABCAM), ADAM10 (1:1000, AB1997, ABCAM), PSEN1 (1:1000, AB76083, ABCAM), and ABCA7 (1:1000, 32942S, Cell Signaling Technology). Membranes were incubated with primary antibodies in tris-buffered saline (TBS) with 0.1% Tween-20 overnight at 4°C with rocking. The following day, membranes were washed in PBS then incubated with secondary antibodies for 1 hour at room temperature. Secondary antibodies and dilutions used were antimouse IRDye 800CW (1:15,000; 926-32210; LI-COR) and antirabbit IRDye 800CW (1:15,000; 926-32211; LI-COR). After

three washes of 5 minutes with TBS-Tween, membranes were imaged using an Odyssey CLx. Quantitative analyses were performed with Empiria Studio Software v2.3 (LI-COR).

2.16 | Generation of ABCA7 overexpressing N2a cells

Mouse N2a neuroblastoma cells were provided by Dr. Masashi Kitazawa (UCI). An empty vector (contains EGFP only, Prp[Exp]-EGFP/neo-CAG > ORF_stuffer), mouse WT ABCA7 (Prp[Exp]-EGFP/neo-CAG > NM_001346081.2), and V1613M ABCA7 (Prp[Exp]-EGFP/neo-CAG > NM_001346081.2*V1613M) were designed and cloned using VectorBuilder (Chicago, IL). Transformed *E. coli* glycerol stocks were propagated, and plasmids purified using Monarch plasmid miniprep kit (T1010S, New England Biolabs, Ipswich, MA). Plasmids were linearized by digestion with *Asc I*, verified by agarose gel electrophoresis, the protein precipitated using 2.5 M ammonium acetate, and plasmid DNA precipitated and sterilized using ethanol. N2a cells were plated into a six-well plate (100,000/well) 24 hours before transfection. Then 2.5 μg plasmid DNA was transfected into the N2a cells using lipofectamine 3000 transfection kit (L3000008, Invitrogen). P3000 was added to increase transfection efficiency. Plasmid DNA and lipofectamine complexes were made in reduced serum media, OptiMEM (31985070, Invitrogen). Complexes were added to cells in 10% fetal bovine serum (FBS) containing DMEM and left for 48 hours before analyzing transfection efficiency via EGFP expression. Selection of positive clones was conducted by selection in G418 (500 μg/mL) for 14 days. Cells were further sorted via FACS buffer to increase the percentage of successfully transfected cells. Transfected cells were maintained in 10% FBS containing DMEM supplemented with 100 μg/mL G418 which was replaced every 3 days.

2.17 | Immunocytochemistry of ABCA7 overexpressing N2a cells

Cells were seeded into 12-well plates (200,000 cells/well) on coverslips in reduced serum media, OptiMEM (31985070, Invitrogen) 24 hours before staining. Cells were washed in 1× PBS (2 × 5 minutes) then fixed in 4% PFA for 20 minutes at room temperature. Following fixation, cells were washed with 1× PBS (3 × 5 minutes) before blocking in 5% normal goat serum supplemented with 0.2% Triton-X, for 1 hour at room temperature. Cells were then incubated with primary antibodies, mouse antimouse APP (1:100; MAB348, MilliporeSigma) and rat antimouse LAMP1 (1:100; AB25245, ABCAM), overnight at 4°C. Cells were subsequently washed with 1× PBS (1 × 10 minutes, 2 × 5 minutes) and incubated with secondary antibodies, antimouse Alexa Fluor 647 (1:200, A-21235, Thermo Fisher Scientific) and antirat Alexa Fluor 555 (1:200, A-21434, Thermo Fisher Scientific), for 1 hour at room temperature. Finally, cells were washed with 1× PBS (1 × 10 minutes, 2 × 5 minutes) and coverslips mounted using Fluoromount-G (0100-01, Southern Biotech). Cells were imaged using LSM 900 (Carl Zeiss) with Airyscan processing (Zen 3.6, Blue edition), 63 × 1.3NA immersion oil objective and 5× digital zoom. Five images were acquired per cell type/stain and APP+ intracellular puncta were counted using ImageJ (Version 1.53t).

2.18 | Statistical analysis

The number of independent biological replicates are indicated by *N* in Figures 1 through 6. The sample sizes are similar to those found in prior studies conducted by MODEL-AD.[25–27] Immunohistochemical and biochemical data were analyzed using a Student *t*-test or two-way ANOVA via Prism v.9 (GraphPad). Tukey's post hoc tests were utilized to examine biologically relevant interactions from the two-way ANOVA. Where sex-differences are apparent, a Student *t*-test was used within the genotype group. Outlier tests were performed via Prism v.9 where relevant and any datapoint removed from the analyses is indicated in the relevant figure legend. Unless otherwise stated, data are presented as raw means and standard error of the mean (SEM).

3 | RESULTS

3.1 | Mouse *Abca7*^{V1613M} allele models human *ABCA7*^{V1599M} allele with no off-target effects

We developed an *Abca7*^{V1613M} mouse model on an inbred C57BL/6J mouse background utilizing previously reported strategies.[27] Sequencing confirmed the desired change on Exon 35 of methionine (M) to valine (V) at amino acid 1613 (Figure 1A). *Abca7* $^{em1\,Aduci}$/J mice are available free of restrictions through The Jackson Laboratory (Stock No. #035316). Bulk RNA sequencing (RNA-seq) analysis of 8-month-old mice indicated relatively few differences in gene expression between WT C57BL/6J mice and *Abca7*^{V1613M} mice, with five genes above the threshold for significance, including reduced expression of *Dok3* which encodes a negative regulator of LPS-induced Toll-like receptor signaling (PMID 22761938) (Figure 1B).[28] Bulk RNA-seq also supports the view that the *Abca7*^{V1613M} allele is expressed at a similar level to the WT *Abca7* allele without evidence of any cryptic splicing products from the modified allele (Figure 1C and data not shown). We confirmed that ABCA7 protein expression is similar in WT and *Abca7*^{V1613M} mice at 4 months of age via western blotting (Figure S2). To further validate the *Abca7*^{V1613M} model we conducted off-target analyses of other putative cut sites within genes or in conserved intergenic regions that might have been targeted by CRISPR-Cas9 during generation of the *Abca7*^{V1613M} allele. *Abca7*^{V1613M} founder mice were backcrossed with WT C57BL/6J animals for three generations before use to generate animals for this study, making it unlikely that a mutation caused by an off-target effect of CRISPR/Cas9 would be present on a chromosome other than chromosome 10, that is, the location of *Abca7* (C57BL/6J; Chr10; 79.8 Mb, GRCm39, Ensembl release 110) (Figure S3). Potential CRISPR/Cas9 off-target sites with up to

four mismatches using crRNA TMF1268 were screened for using Cas-OFFinder (http://www.rgenome.net/cas-offinder/;). Nineteen potential off-target sites on mouse chromosome 10 were identified (Table S1). Five potential off-target sites were within introns and three were located within conserved intergenic regions while the remaining eleven were within nonconserved intergenic regions. To screen for evidence of CRISPR/Cas9 RNP activity at the intronic and conserved intergenic sites, DNA from a WT and two homozygous *Abca7*^{V1613M} mice were amplified by PCR using the primers listed (Table S2), then sequenced across the potential off-target region at each locus. None of the eight potential off-target sites analyzed showed a difference in sequence between WT and homozygous *Abca7*^{V1613M} mice (Figure S3). These data suggest that selective mutagenesis of mouse *Abca7* at amino acid position 1613 was successful with no unwanted off-target effects. Furthermore, introduction of this missense variant does not change expression of ABCA7 at the RNA or protein level, suggesting that any phenotypic changes seen in animals with this variant are due to differences in ABCA7 function, not expression.

3.2 | Homozygous *Abca7*^{V1613M} mice display a differential response to LPS challenge and increased microglial phagocytosis

Previous studies implicate a role for ABCA7 in inflammation and microglial function,[15,17] but the effects of the V1599M/V1613M variant are unknown, including whether it behaves as a loss of function variant. *Abca7* haploinsufficient mice display diminished responses to LPS stimulation.[17] To investigate the impact of the V1613M variant on the brain's ability to mount an immune response to immune challenge, we injected 8-month-old C57BL/6J (WT) and homozygous *Abca7*^{V1613M} mice intraperitoneally with saline or 0.3 mg/kg LPS and collected brains for bulk tissue RNA-seq analysis at 6 and 24 hours postinjection. LPS administration induces a robust inflammatory response in both in WT (Figure 1E) and *Abca7*^{V1613M} (Figure 1F) animals at 6 hours postinjection, as indicated by increased transcription of inflammatory genes such as *Ccl2*, *Cxcl1*, *Il1b*, and *Tnfa*, accompanied by downregulation of the homeostatic microglial gene, *P2ry12*. Specifically, there are 273 upregulated and 101 downregulated genes in WT LPS versus saline at 6 hours and 325 upregulated and 51 downregulated genes in *Abca7*^{V1613M} LPS versus saline at 6 hours (Figure 1E,F). To identify LPS-dependent DEGs in *Abca7*^{V1613M} mice, we compared *Abca7*^{V1613M} LPS-treated versus *Abca7*^{V1613M} saline-treated, and *Abca7*^{V1613M} LPS-treated versus WT LPS-treated mice at 24 hours postinjection and found 88 overlapping genes (Figure 1K). Of these 88 genes, the majority are upregulated in *Abca7*^{V1613M} mice compared to WT at both 6 and 24 hours postinjection (Figure 1L). Of note, *Abca7*^{V1613M} mice do not fully resolve LPS-induced gene expression changes by 24 hours postinjection and have upregulation of a large number of inflammatory-associated genes such as *C1ra*, *C1qa*, *C1qb*, *Casp4*, and *Capg* compared to their WT counterparts (Figure 1H,I). Pathway analyses of these 88 genes reveal a high association with interferon signaling and classical complement/inflammatory signaling pathways. Given these changes in the central nervous system, we next explored the plasma response to LPS. *Abca7*^{V1613M} mice had similar or lower levels of most cytokines analyzed, including IFN-γ, IL-6, and TNFα, when compared to WT animals 24 hours postinjection (Figure S4). These data indicate that homozygous *Abca7*^{V1613M} mice evoke a differential response to LPS stimulation compared to WT animals, which appears to be specific in the brain and not due to augmentation of LPS-mediated peripheral cytokine levels. Together, these findings indicate that *Abca7*^{V1613M} mice are less able to resolve LPS-induced brain-associated inflammation and/or remain more activated after challenge. These data are in contrast to previous studies using *Abca7* haploinsufficient mice, in which inflammation was suppressed.

We analyzed the in vitro phagocytic capacity of microglia isolated from cortices of *Abca7*^{V1613M} homozygous and WT control p3- to 5-day-old mice. Primary microglia were incubated with either carboxylated fluorescent beads, which mimics uptake of dead/dying cells, or fluorescently labelled Aβ1-42 peptide for 1 hour before uptake was analyzed via flow cytometry (Figure 1M). Microglia from *Abca7*^{V1613M} mice have increased phagocytic capacity of both beads and Aβ1-42 peptide compared to WT controls (Figure 1N,O). These data also contrast with previous studies that report reduced phagocytosis of apoptotic cells and Aβ oligomers in *ABCA7* KO macrophages and microglia.[15–17] Together, these data suggest that the V1613M variant in murine *Abca7* produces a gain of function (hypermorphic or neomorphic) effect with respect to inflammation and microglial phagocytosis, and not a loss of function.

3.3 | *Abca7*^{V1613M} mediates distinct changes in the lipid profile of 5xFAD mice

To explore the impact of the *Abca7*^{V1613M} variant in the context of plaque development, and its effects on the brain we crossed *Abca7*^{V1613M} mice with the 5xFAD mouse model of amyloidosis to generate four experimental genotypes, C57BL/6J (WT), *Abca7*^{V1613M} homozygous (*Abca7*^{V1613M}), 5xFAD hemizygous (5xFAD HEMI), and 5xFAD/*Abca7*^{V1613M}. All mice were inbred or co-isogenic C57BL/6J background. Cohorts of mice of both sexes and each genotype were aged to 4 and 12 months of age to reflect early and late stages of pathology, respectively (Figure 2A).

ABCA7 is a lipid transporter predominantly involved in cholesterol/phospholipid efflux and *Abca7* KO mice have altered lipid profiles.[9,11,12,14,29] Because dyslipidemia can be related to weight[30] we measured animal total body weight. Twelve-month-old WT and *Abca7* ^{V1613M} animals have similar mass (Figure 2B). In contrast, 12-month-old 5XFAD mice have reduced body weight compared to 5XFAD/*Abca7*^{V1613M}, WT, and homozygous *Abca7*^{V1613M} animals (Figure 2B), indicating a protective effect of the *Abca7*^{V1613M} variant against 5xFAD-mediated weight loss.

We next examined the impact of the *Abca7*^{V1613M} variant on lipid homeostasis by analyzing plasma and cortical tissue from WT, *Abca7*^{V1613M}, 5xFAD, and 5xFAD/*Abca7*^{V1613M} mice of both sexes and 12 months of age. We quantified circulating plasma lipids including

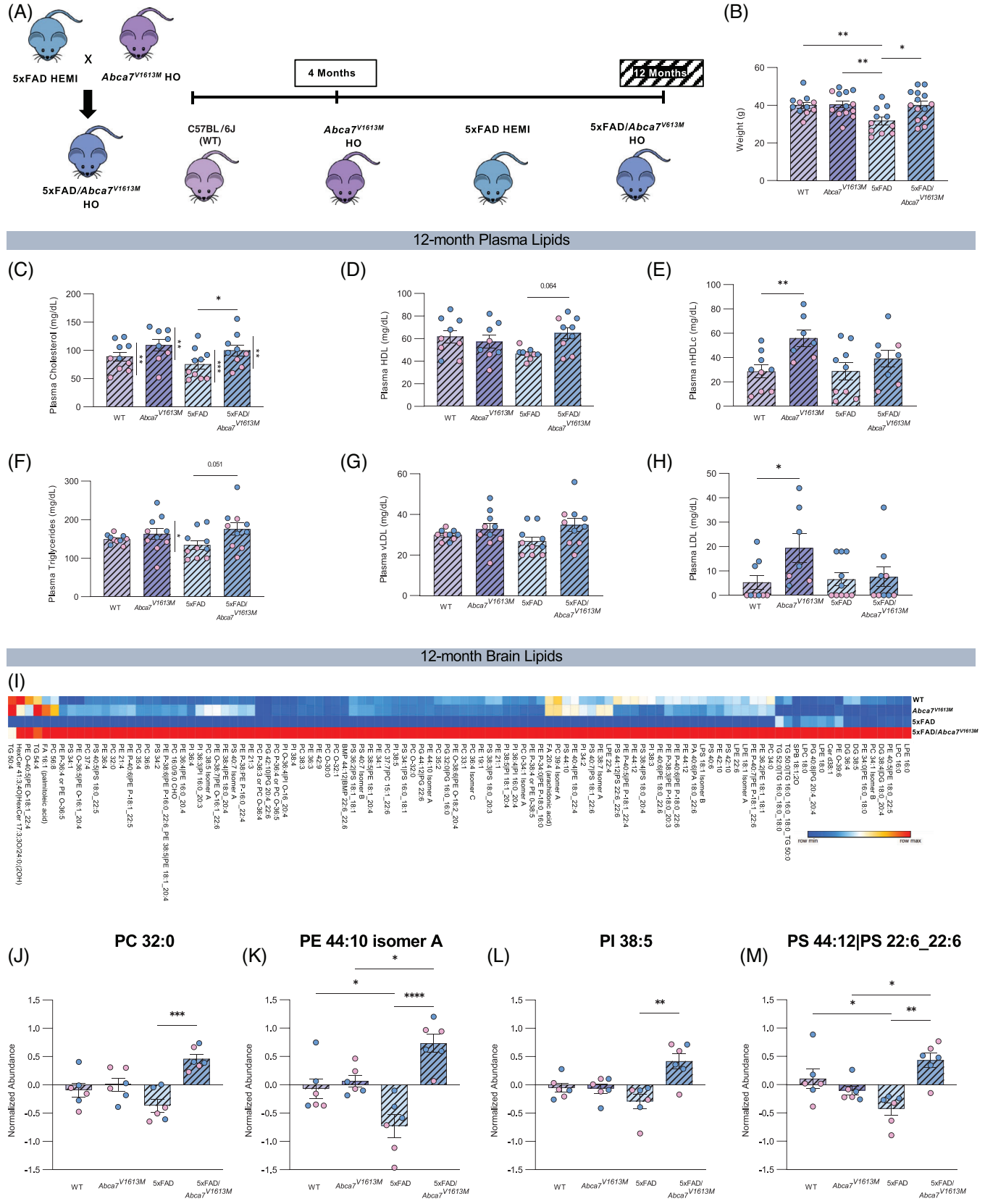

FIGURE 2 Altered plasma and brain lipids in 12-month-old 5xFAD/*Abca7*^{V1613M} mice. (A) Schematic demonstrating the initial cross used to generate the desired genotypes and the timepoints used in this study. All data in this figure are from the 12-month timepoint. (B) Weight of mice from all four experimental groups at 12 months of age. (C-H) Analysis of the effect of the *Abca7*^{V1613M} variant on circulating lipids in plasma in 12-month-old mice. Quantification of (C) total cholesterol, (D) high-density lipoprotein (HDL), (E) non- HDL cholesterol (nHDLc), (F) triglycerides, (G) very low-density lipoprotein (vLDL), (H) LDL. $N = 3$ to 6 per sex/genotype/age. Statistically significant differences between sexes are denoted

CHOL, HDL, and triglycerides. In plasma, 5xFAD/*Abca7*^{V1613M} mice have increased CHOL compared to 5xFAD mice (Figure 2C). Male mice have higher CHOL levels compared to females in all genotypes (Figure 2C). *Abca7*^{V1613M} mice trended to have increased cholesterol compared to WT mice (Figure 2C). We report a statistically significant effect of genotype on cholesterol levels ($F = 6.336$ and $p = 0.0026$), suggesting the V1613M variant has an effect on levels of circulating cholesterol. 5xFAD/*Abca7*^{V1613M} have higher levels of plasma HDL (Figure 2D) and triglycerides (Figure 2F) compared to 5xFAD mice, with differences close to statistical significance. In the absence of the 5xFAD transgene, *Abca7*^{V1613M} mice show increased plasma nHDLc (Figure 2E) and LDL (Figure 2H) compared to WT controls. No difference was detected in plasma vLDL across genotypes (Figure 2G). These data indicate ABCA7-dependent roles in circulating cholesterol homeostasis, and a differential role with the introduction of the *Abca7*^{V1613M} variant.

To assess lipid changes in the brain, we performed unbiased bulk lipidomics on cortical tissue using liquid chromatography-mass spectrometry. ANOVA revealed significant difference in lipid abundance between the groups for 106 of 552 identified lipids ($p < 0.05$) comprising a range of species, mostly phosphatidylcholines (PCs), phosphatidylethanolamines (PEs), phosphatidylinositols (PIs), and phosphatidylserines (PSs), shown as a heatmap (Figure 2I). Of these 106 lipids we plotted several key metabolites, PC 32:0, PE 44:10 isomer A, PI 38:5, and PS 44:12|PS 22:6_22:6 (Figure 2J–M), to highlight differences between all four groups. There is a consistent increase in the levels of lipids in 5xFAD/*Abca7*^{V1613M} mice compared to 5xFAD controls.

3.4 | *Abca7*^{V1613M} reduces Aβ plaque pathology in 5xFAD mice

Loss of ABCA7 exacerbates Aβ plaque pathology in APP-overexpressing mice.[12,19] To investigate the effect of the *Abca7*^{V1613M} variant on development of plaque pathology, coronal brain sections from 5xFAD and 5xFAD/*Abca7*^{V1613M} mice were stained with ThioS and a conformation-specific antibody (Aβ fibrils OC) to evaluate amyloid plaque and fibrillar Aβ deposition, respectively. 5xFAD mice homozygous for the *Abca7*^{V1613M} variant have fewer ThioS+ plaques in the cortex and hippocampus at both 4 and 12 months of age (Figure 3C–H, K–Q). OC+ staining is also reduced in both the cortex and subiculum at 4 months and in the cortex at 12 months (Figure 3E–J, N–S). Hence, the *Abca7*^{V1613M} variant appears to have the opposite effect on development of Aβ plaque compared to mice with a complete loss of function of *Abca7*.

3.5 | *Abca7*^{V1613M} reduces Aβ-associated neuronal damage but does not affect synapse loss in 5xFAD mouse model

Aβ deposition is known to be associated with neuronal damage and neurodegeneration, as seen by the formation of dystrophic neurites, elevated NfL in plasma and cerebral spinal fluid, as well as loss of synapses.[31–33] To assess whether the reduction in Aβ in *Abca7*^{V1613M} mice was associated with reduced damage and neurodegeneration in the 5xFAD brain, we examined dystrophic neurites in 5xFAD and 5xFAD/*Abca7*^{V1613M} mice, as well as synapses via immunohistochemistry and NfL via MSD assay in all four groups. Brain sections were stained with ThioS and LAMP1, a marker for dystrophic neurites. At 4 and 12 months of age there is a large reduction in total LAMP1 staining in the cortex, although this reduction is only significant at 4 months in the subiculum between 5xFAD and 5xFAD/*Abca7*^{V1613M} mice (Figure 4A–F). The reduced LAMP1 correlates well with the reduced Aβ plaques in the brain. Similarly, a significant and sustained reduction in NfL was observed in both plasma and cortex in 5xFAD/*Abca7*^{V1613M} mice compared to 5xFAD controls at both ages analyzed (Figure 4G–J).

We investigated whether the *Abca7*^{V1613M} variant affected synaptic density by quantifying the presynaptic marker BASSOON, and postsynaptic marker HOMER1 in the 12-month cohort. There were fewer BASSOON spots in the CA1 region of hippocampus in 5xFAD mice compared to WT controls (Figure 4P). However, no difference was found between 5xFAD and 5xFAD/*Abca7*^{V1613M} animals (Figure 4P). In cortex and subiculum no difference was found in the number of BASSOON spots between all groups (Figure 4L–O). There was no significant difference in HOMER1 spots in any of the brain region images, except for a minor reduction in HOMER1 spots in the subiculum between *Abca7*^{V1613M} homozygous mice with pathology versus those without (Figure 4O).

Together, these data indicate that the 5xFAD/*Abca7*^{V1613M} mice have reduced neuron-associated damage, consistent with less Aβ pathology. Additionally, the V1613M variant does not influence plaque induced synaptic loss, or synapse densities under homeostatic conditions.

3.6 | *Abca7*^{V1613M} reduces Aβ-associated gliosis in 4-month-old 5xFAD mice

Microglia are implicated in the pathology of AD and are found in close proximity and actively react to Aβ plaques, inducing distinct transcriptional changes.[34] To analyze the effect of the *Abca7*^{V1613M} variant

by vertical bars and associated significance markers. (I-M) Liquid chromatography/mass spectrometry analysis of cortical brain lipids in 12-month-old mice. (I) Heatmap of significantly altered lipids identified by analysis of variance (ANOVA). (J-M) Normalized abundance of (J) phosphatidylcholine (PC) 32:0, (K) phosphatidylethanolamine (PE) 44:10 isomer A, (L) phosphatidylinositol (PI) 38:5, (M) phosphatidylserine (PS) 44:12|PS 22:6_22:6. $N = 6$ per genotype. Data are represented as mean ± SEM. Statistics (B-H, J-M) by two-way ANOVA. WT, wildtype. $^{*}p \leq 0.05$, $^{**}p \leq 0.01$ $^{***}p \leq 0.001$, $^{****}p \leq 0.0001$.

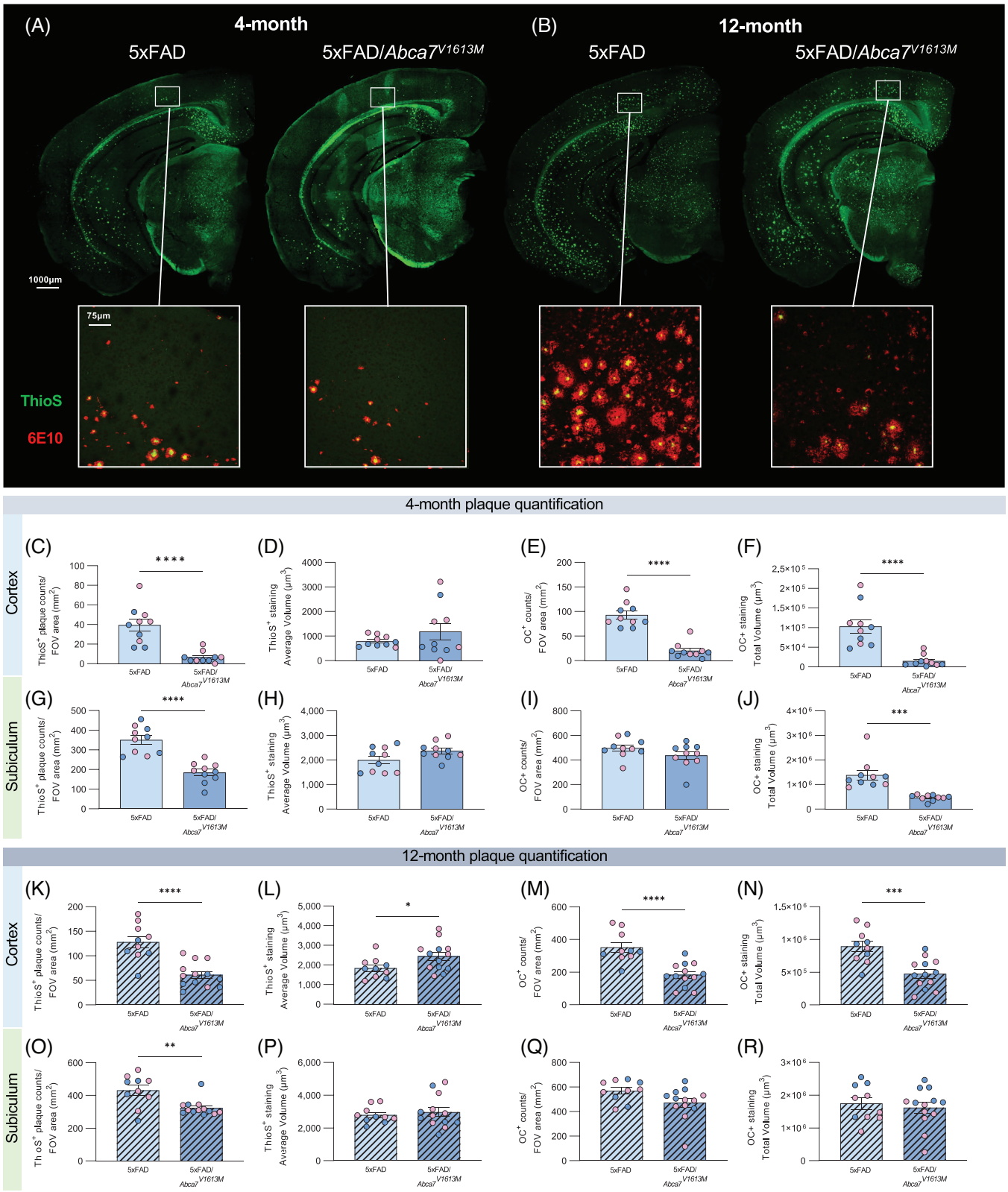

FIGURE 3 Reduced amyloid beta (Aβ) plaque burden in 5xFAD/*Abca7*^{V1613M} mice. Plaque burden in 4- and 12-month-old 5xFAD hemizygous (5xFAD), and 5xFAD hemizygous /*Abca7*^{V1613M} homozygous (5xFAD/*Abca7*^{V1613M}) animals was assessed with Thioflavin S (ThioS) and OC staining. (A-B) Representative hemispheric brain and higher magnification cortical images from 5xFAD and 5xFAD/*Abca7*^{V1613M} females showing ThioS+ dense core plaques and more fibrillar OC staining at (A) 4 months and (B) 12 months. (C-R) Quantification of (C) ThioS+ plaques in cortex at 4 months, (D) average volume of ThioS+ plaques in cortex at 4 months, (E) OC+ plaques in cortex at 4 months, (F) total volume of OC+ staining in cortex at 4 months, (G) ThioS+ plaques in subiculum at 4 months, (H) average volume of ThioS+ plaques in subiculum at 4 months, (I) OC+ plaques

on the plaque–microglial association in 5xFAD mice, we stained for microglia with IBA1, and Aβ plaques with ThioS, in both brain regions at 4 and 12 months. 5xFAD/ *Abca7*^{V1613M} mice have reduced microglial density in the cortex and subiculum at both 4 and 12 months of age (Figure 5B, D, G, I) compared to 5xFAD, although no difference was observed in the number of microglia associated per Aβ plaque in both regions and timepoints (Figure 5C, E, H, J).

To identify changes in gene expression associated with homozygosity for the *Abca7*^{V1613M} variant in 5xFAD mice we conducted bulk tissue RNA-seq on hippocampi. Consistent with the reduced plaque load in 4-month-old 5xFAD/*Abca7*^{V1613M} mice, we found reduced transcripts for inflammatory/microglial expressed genes such as *Cst7*, *Trem2*, *Itgax*, and *Hexb* in 5xFAD/*Abca7*^{V1613M} mice compared with 5xFAD animals (Figure 5K). By contrast, in 12-month-old animals, despite lower plaque loads, we did not identify any differentially expressed genes between 5xFAD/*Abca7*^{V1613M} and 5xFAD mice (Figure 5L). However, there were sustained reductions in TPMs of disease-associated microglia genes when considered individually: *Ctsd*, *Cst7*, and *Itgax* (Figure 5Q–S). We confirmed the reduction in *Itgax* at the protein level by analyzing CD11c via immunohistochemistry in hippocampi of 12-month-old animals (Figure S5). To further explore gene expression changes across groups, we analyzed functional networks of correlated genes (WGCNA) and identified one module which contains inflammation/immune-related genes that are highly upregulated in 5xFAD mice but significantly reduced in 5xFAD/*Abca7*^{V1613M} mice. We plotted eigengene values of these inflammation module for all groups (Figure 5M), revealing a reduction in 5xFAD/*Abca7*^{V1613M} mice compared to 5xFAD at both 4 and 12 months of age.

We also explored astrocytic responses to plaques through immunohistochemistry for GFAP, a general marker of activation, and S100β, which stains most astrocytes regardless of activation state, in both regions and timepoints. At the 4- and 12-month timepoints there is reduced total volume of GFAP+ astrocytes in the cortex and subiculum in 5xFAD/*Abca7*^{V1613M} mice compared to 5xFAD controls (Figure S6B, D, G, I), with no change in the number of S100β + astrocytes in the cortex (Figure S6C, H). Immunohistology GFAP data in the subiculum are consistent with reduced GFAP TPM values in 5xFAD/*Abca7*^{V1613M} mice compared to 5xFAD at both 4 and 12 months of age from bulk RNA-seq analysis of hippocampi (Figure S6K). In the subiculum at 4 months there is a small but significant reduction in the number of S100β+ astrocytes between 5xFAD/*Abca7*^{V1613M} and 5xFAD mice, which is no longer significant at 12 months of age (Figure S6E, J).

Collectively, these data indicate that 5xFAD/*Abca7*^{V1613M} mice exhibit reduced microgliosis and inflammation, which is likely due to lower Aβ plaque burden compared to 5xFAD controls rather than distinct changes to microglial gene expression and function.

3.7 | *Abca7*^{V1613M} results in altered APP processing and trafficking but does not affect cholesterol efflux in vitro

Prior studies suggested that ABCA7 KO could mediate increased plaque burden through impairment in microglial clearance of Aβ.[12,17] However, we found no overt difference in microglial response to plaques in 5xFAD/*Abca7*^{V1613M} mice when normalized for the reduction in plaque load. We postulated that the effect of the Abca7^{V1613M} variant on plaques might instead be due to altered Aβ production. To test this theory, we quantified Aβ40 and Aβ42 in both the detergent insoluble and soluble fractions representing Aβ sequestered in plaques versus that being actively produced, respectively, from hippocampal and cortical tissue. Consistent with plaque analysis, we observed reduced Aβ40 and Aβ42 in the insoluble and soluble fractions of the cortex and hippocampus at 4 months in 5xFAD/*Abca7*^{V1613M} mice compared to 5xFAD controls (Figure 6A–H). Broadly, Aβ levels are also reduced at 12 months in both the soluble and insoluble fractions in 5xFAD/*Abca7*^{V1613M} compared to 5xFAD mice (Figure 6I–P). Together, these data suggest that *Abca7*^{V1613M} reduces Aβ production, and that this results in less Aβ sequestered in plaques.

Aβ is sequentially cleaved from its parent protein, APP, by BACE1 followed by the γ-secretase complex. We conducted western blot analysis of key enzymes and products of the APP processing pathway: full-length APP, C-terminal APP fragments C83 and C99, BACE-1 (β-secretase), PSEN1 (component of the γ-secretase complex), and ADAM-10 (α-secretase). 5xFAD/*Abca7*^{V1613M} mice have reduced full-length APP and corresponding C terminal fragments (C83 and C99) (Figure 6Q, R). However, there was no difference in BACE1, PSEN1, or ADAM10 between 5xFAD and 5xFAD/*Abca7*^{V1613M} animals (Figure 6Q, R). Uncropped versions of these blots can be found in Figure S7. These data suggest that reduced Aβ generation and subsequent plaque development are due to changes in the proteolytic cleavage of both α- and β-secretases (ADAM10 and BACE1, respectively), possibly reflecting a change in the availability of the substrate (ie, APP).

We hypothesized that the *Abca7*^{V1613M} variant was altering intracellular APP trafficking, such that it was less available for α- or β-secretase cleavage. To test this theory, we generated N2a cell lines overexpressing either WT ABCA7 or V1613M-ABCA7 and evaluated the subcellular localization of APP via super resolution microscopy. First, to assess whether Aβ levels were reduced in N2a cells overexpressing WT ABCA7 or V1613M-ABCA7, we measured Aβ40 and Aβ42 in both the supernatant and cell lysate of all four cell lines. We found a reduction of both Aβ40 and Aβ42 in the supernatant and lysate of N2a cells overexpressing WT and V1613M-ABCA7 compared to nontransfected and EGFP-only (empty vector) control lines

in subiculum at 4 months, (J) Total volume of OC+ staining in subiculum at 4 months, (K) ThioS+ plaques in cortex at 12 months, (L) average volume of ThioS+ plaques in cortex at 12 months, (M) OC+ plaques in cortex at 12 months, (N) total volume of OC+ staining in cortex at 12 months, (O) ThioS+ plaques in subiculum at 12 months, (P) average volume of ThioS+ plaques in subiculum at 12 months, (Q) OC+ plaques in subiculum at 12 months, (R) total volume of OC+ plaques in subiculum at 12 months. $N = 4$ to 6 per sex/genotype/age. Data are represented as mean ± SEM. Statistics (C-S) by unpaired Student *t*-test. FOV, field of view. $^{*}p \leq 0.05$, $^{**}p \leq 0.01$, $^{***}p \leq 0.001$, $^{****}p \leq 0.0001$.

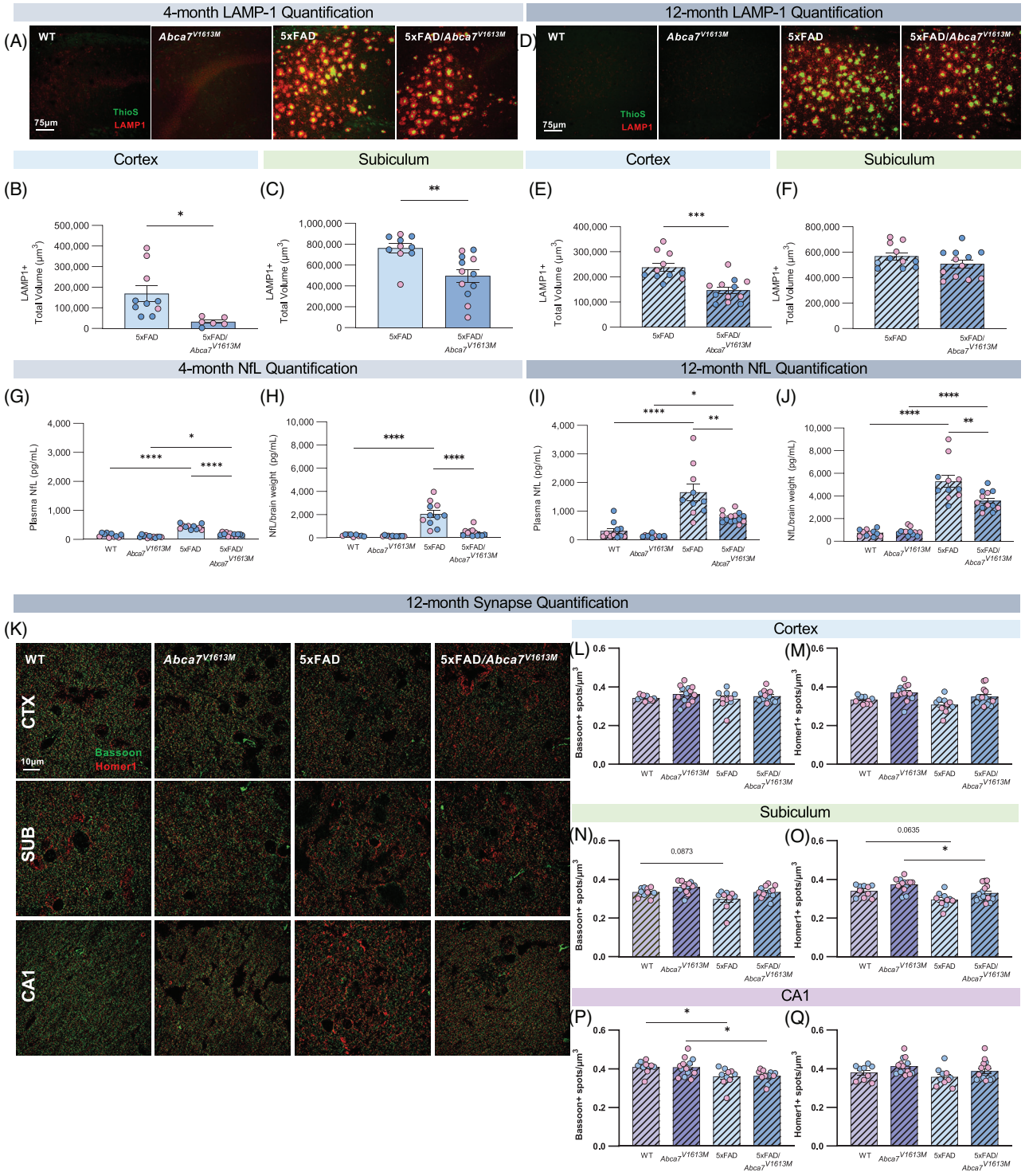

FIGURE 4 5xFAD/*Abca7*^{V1613M} mice have reduced amyloid beta (Aβ)-associated neuronal damage. (A) Representative confocal images of subiculum in 4-month-old wildtype (WT), *Abca7*^{V1613M}, 5Xfad, and 5xFAD/*Abca7*^{V1613M} mice stained with Thioflavin S (ThioS; green) and LAMP1 (red). Scale bar = 75 microns. (B-C) Quantification of total LAMP1+ staining in (B) cortex and (C) subiculum at 4 months of age. (D) Representative confocal images of subiculum in 12-month-old WT, *Abca7*^{V1613M}, 5xFAD, and 5xFAD/*Abca7*^{V1613M} mice stained with ThioS (green) and LAMP1 (red). Scale bar = 75 microns. (E-F) Quantification of total LAMP1+ staining in (E) cortex and (F) subiculum at 12 months of age. (G-J) Compared with 5xFAD mice, 5xFAD/*Abca7*^{V1613M} animals display lower neurofilament light chain (NfL) in plasma and cortex at 4 and 12 months of age. (K) Representative super resolution images of synaptic densities in different sites in 12-month-old WT, *Abca7*^{V1613M}, 5xFAD, and 5xFAD/*Abca7*^{V1613M} mice. Scale bar = 10 microns. (L-Q) Quantification of (L) presynaptic BASSOON spots and (M) postsynaptic HOMER1 spots normalized to volume of z stack in cortex; (N) presynaptic BASSOON spots and (O) postsynaptic HOMER1 spots normalized to volume of z stack in subiculum; and (P) presynaptic BASSOON spots and (Q) postsynaptic HOMER1 spots normalized to volume of z stack in CA1. $N = 4$ to 6 per sex/genotype/age. Data are represented as mean ± SEM. Statistics (B-F) by unpaired Student *t*-test, (G-Q) by two-way analysis of variance. $^{*}p \leq 0.05$, $^{**}p \leq 0.01$, $^{***}p \leq 0.001$, $^{****} \leq 0.0001$.

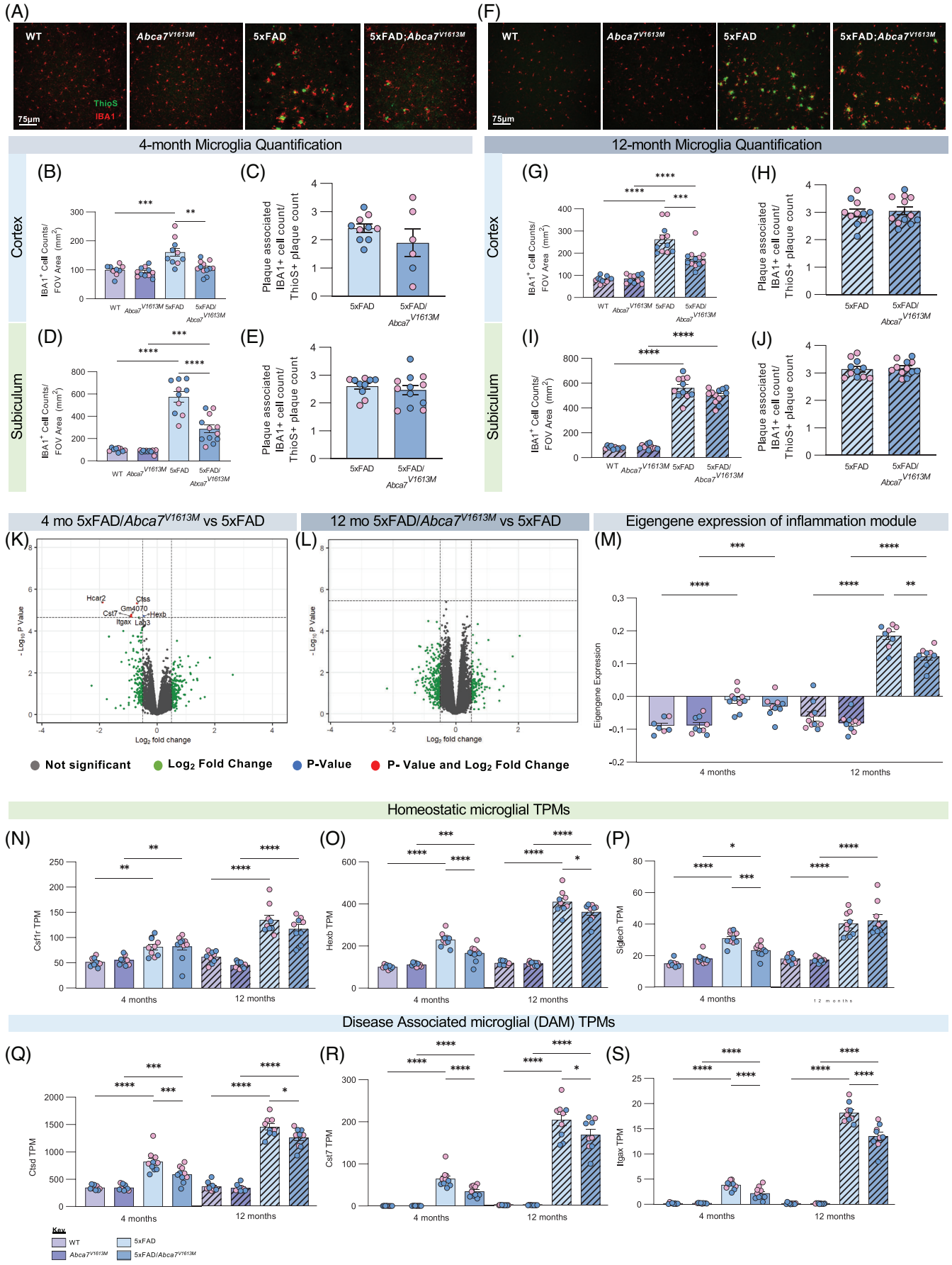
(A)
WT
Abca7V1613M
5xFAD
5xFAD;Abca7V1613M
ThioS
IBA1
75μm
(F)
4-month Microglia Quantification
12-month Microglia Quantification
Cortex
Subiculum
(B)
(C)
(D)
(E)
(G)
(H)
(I)
(J)
IBA1+ Cell Counts/ FOV Area (mm2)
Plaque associated IBA1+ cell count/ ThioS+ plaque count
4 mo 5xFAD/Abca7V1613M vs 5xFAD
12 mo 5xFAD/Abca7V1613M vs 5xFAD
Eigengene expression of inflammation module
(K)
(L)
(M)
- Log10 P Value
Log2 fold change
Hcar2
Ctss
Gm4070
Cst7
Hexb
Itgax
Lag3
Eigengene Expression
4 months
12 months
Not significant
Log2 Fold Change
P-Value
P- Value and Log2 Fold Change
Homeostatic microglial TPMs
(N)
(O)
(P)
Csf1r TPM
Hexb TPM
Siglech TPM
Disease Associated microglial (DAM) TPMs
(Q)
(R)
(S)
Ctsd TPM
Cst7 TPM
Itgax TPM
Key
WT
Abca7V1613M
5xFAD
5xFAD/Abca7V1613M

(Figure S8D–G). These data are consistent with our in vivo findings that show a reduction in Aβ40 and Aβ42 in 5xFAD/*Abca7*^{V1613M} mice compared to 5xFAD controls. N2a cells overexpressing mouse WT ABCA7 exhibited a small number of APP-positive intracellular puncta (average of 3 per cell) (Figure 6S, V). We also see these puncta in non-transfected and EGFP-only controls but at a much lower frequency (average of one punctum per cell) (Figure 6S, T, U). N2a cells overexpressing V1613M-ABCA7 display significantly increased intracellular APP puncta (average seven puncta per cell) compared to WT ABCA7 overexpressing and control cells (Figure 6S, W). To assess whether overexpression of WT or V1613M-ABCA7 could be associated with changes in APP trafficking we stained N2a cells with LAMP1, a marker for both lysosomes and late endosomes, and RAB7A, a marker for late endosomes and SXN4, a marker for sorting/recycling endosomes. We found that APP puncta colocalized with LAMP1+ and RAB7A+ structures (Figure 6W, Figure S8H) but not with SNX4 (Figure S8I). These data suggest overexpression of ABCA7 alters APP trafficking by promoting intracellular accumulation in LAMP1+ and RAB7+ structures, and that the V1613M variant enhances this effect. This intracellular accumulation suggests APP is being retained/degraded in the lysosomal pathway rather than being recycled back to the cell membrane, thereby leading to a reduction in Aβ production.

Given differences in circulating cholesterol levels with introduction of the V1613M variant, we conducted a cholesterol efflux assay on our WT and V1613M overexpressing N2a cells, along with their controls. We found no statistical significance in cholesterol efflux between control cells and WT or V1613M ABCA7 overexpressing N2a cells (Figure S8K).

4 | DISCUSSION

GWAS of AD and control individuals identified variants associated with the *ABCA7* locus as having increased risk of development of LOAD.[5,35] More recently, exome sequencing of *ABCA7* identified nonsense and missense coding variants that are predicted to affect protein structure and function. Many of these identified changes appear likely to result in loss of function mutations and have been found to be enriched in AD individuals.[4,20,21,36–39,40–42] Consistent with this finding, results of expression studies that indicate that AD brains with low levels of ABCA7 develop AD at a younger age than those with higher expression of ABCA7, while individuals who expressed ABCA7 at similar levels to healthy controls developed AD at a very late age.[43,44] To date, only one protective low frequency coding missense variant has been identified (rs72973581, p.G215S) and has been hypothesized to induce a small gain of function or increase in ABCA7 expression, although this has not yet been confirmed.[21] Together, these findings suggest that reduced function of ABCA7 may be an important risk factor in the development of AD.[44]

Investigating the ability of disease-associated SNPs to modulate brain function and aging to promote or protect against the development of AD is important to build testable models to understand mechanisms of the disease. We evaluated the V1599M (V1613M in mouse) coding variant for potential inclusion into new LOAD models due to its location within a relatively well conserved region of homology between mouse and human ABCA7 and due to its prediction to be a deleterious mutation, thereby potentially acting as a loss of function mutation, which has been linked to worsening of AD-relevant pathologies.[4,21,36,39,40] Notably, our results here are inconsistent with the actions of a variant that would increase risk for the development of AD, with profound reductions in both Aβ and plaques seen with *Abca7*^{V1613M}. Consistent with this, recent findings suggest the V1599M variant does not confer risk for AD.[4,21,45–48] It is important to note that the bar for proving protection against AD risk is higher, and it is established that the variant is present in centenarians, and therefore does not preclude extreme aging.[47] Larger studies incorporating more V1599M carriers may help to clarify whether this variant confers protection against AD risk.

Single-cell transcriptional and western analysis has shown that *Abca7* is expressed at comparable levels in all cell types of the murine brain.[19,49] In the human brain, *ABCA7* expression is relatively low under physiological conditions[50] and like mice, is also expressed at similar levels in all cell types.[51–54] ABCA7 is a member of the ABC superfamily and is thought to be a key regulator of lipid efflux, phagocytosis, and

FIGURE 5 5xFAD/*Abca7*^{V1613M} mice display reduced microgliosis at 4 and 12 months. Microglia number and size were assessed by staining coronal sections with IBA1 at 4 and 12 months. (A) Representative confocal images from cortex of wildtype (WT), *Abca7*^{V1613M} homozygous, 5Xfad, and 5XFAD/*Abca7*^{V1613M} mice displaying reduced number of microglia at 4 months. Scale bar = 75 microns. (B) IBA1+ cell density in cortex at 4 months. (C) Quantification of IBA1+ cells associated with Thioflavin S (ThioS)+ plaque in cortex at 4 months. (D) IBA1+ cell density in subiculum at 4 months. (E) Quantification of IBA1+ cells associated with ThioS+ plaque in subiculum at 4 months. (F) Representative confocal images from cortex of WT, *Abca7*^{V1613M} homozygous, 5xFAD, and 5XFAD/*Abca7*^{V1613M} mice displaying reduced number and size of microglia at 12 months. Scale bar = 75 microns. (G) IBA1+ cell density in cortex at 12 months. (H) Quantification of IBA1+ cells associated with ThioS+ plaque in cortex at 12 months. (I) IBA1+ cell density in subiculum at 12 months. (J) Quantification of IBA1+ cells associated with ThioS+ plaque in subiculum at 12 months. (K,L) Volcano plots of bulk RNA-seq displaying differentially expressed genes (DEGs) between 5xFAD/*Abca7*^{V1613M} versus 5xFAD at (K) 4 and (L) 12 months of age. (M) inflammatory module eigengene values in WT, *Abca7*^{V1613M} homozygous, 5Xfad, and 5XFAD/*Abca7*^{V1613M} mice at 4 and 12 months of age. Results indicate reduced expression of inflammatory genes in 5xFAD/*Abca7*^{V1613M} mice compared to 5xFAD. (N-S) Transcripts per million (TPMs) of homeostatic markers (N) *Csf1r*, (O) *Hexb*, and (P) *Siglech*; and of disease-associated microglia (DAM) markers (Q) *Ctsd*, (R) *Cst7*, and (S) *Itgax*. A Log_2 fold change of 0.5 was used for all volcano plots; however, $-\text{Log}_{10}$ *p*-value changed according to different comparisons analyzed. $N = 4$ to 6 per sex/genotype/age. Data are represented as mean ± SEM. Statistics (B,D,G,I) by two-way analysis of variance (ANOVA), (C,H,E,J) by unpaired Student *t*-test, (M-S) by two-way ANOVA on 4 or 12 months separately. FOV, field of view. $^{*}p \leq 0.05$, $^{**}p \leq 0.01$, $^{***}p \leq 0.001$, $^{****} \leq 0.0001$.

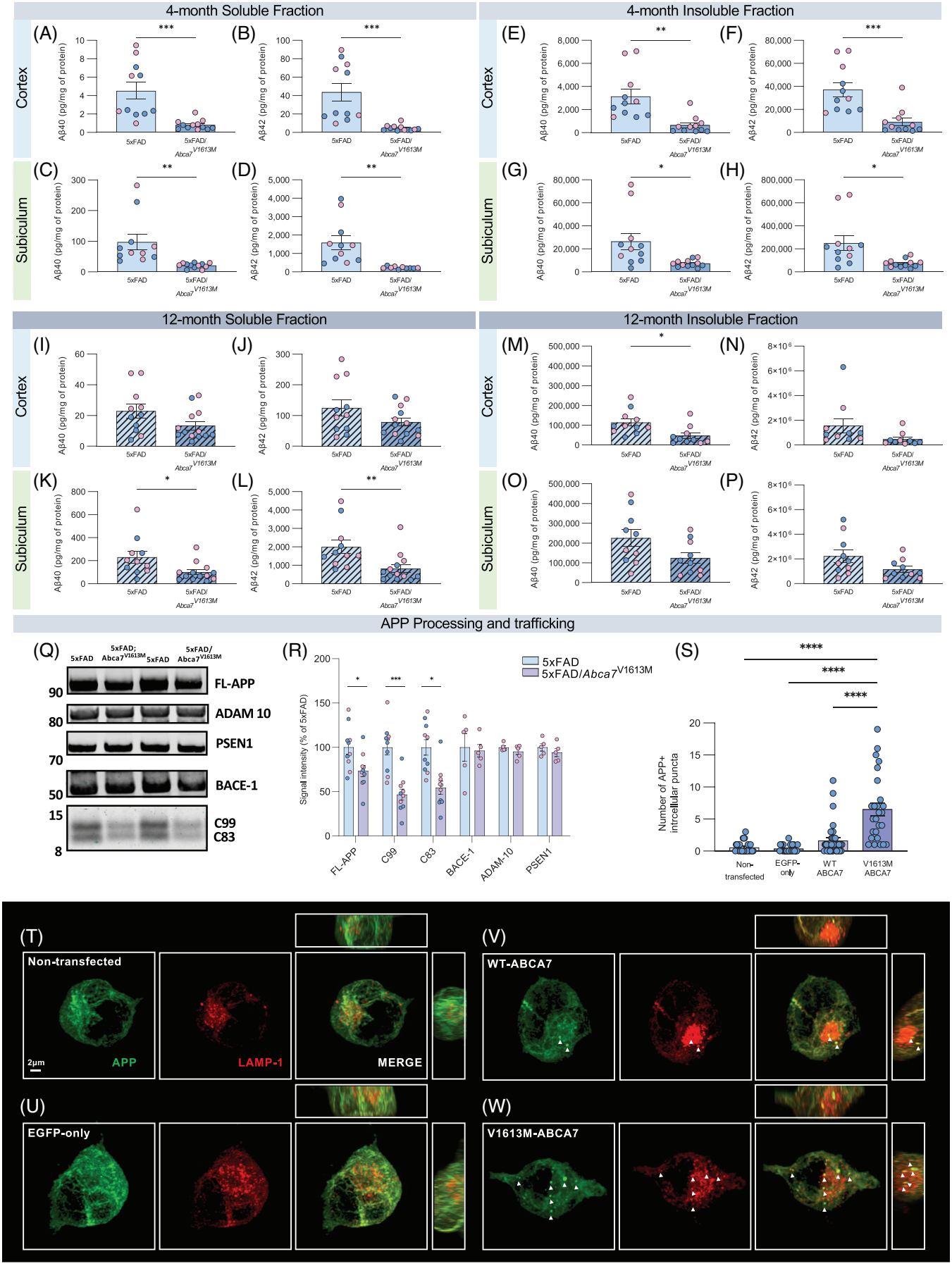
4-month Soluble Fraction
4-month Insoluble Fraction
12-month Soluble Fraction
12-month Insoluble Fraction
Cortex
Subiculum
(A)
(B)
(C)
(D)
(E)
(F)
(G)
(H)
(I)
(J)
(K)
(L)
(M)
(N)
(O)
(P)
Aβ40 (pg/mg of protein)
Aβ42 (pg/mg of protein)
5xFAD
5xFAD/ Abca7V1613M
APP Processing and trafficking
(Q)
5xFAD
5xFAD; Abca7V1613M
5xFAD
5xFAD/ Abca7V1613M
FL-APP
ADAM 10
PSEN1
BACE-1
C99
C83
(R)
5xFAD
5xFAD/Abca7V1613M
Signal intensity (% of 5xFAD)
FL-APP
C99
C83
BACE-1
ADAM-10
PSEN1
(S)
Number of APP+ intrcellular puncta
Non-transfected
EGFP-only
WT ABCA7
V1613M ABCA7
(T)
Non-transfected
APP
LAMP-1
MERGE
2μm
(V)
WT-ABCA7
(U)
EGFP-only
(W)
V1613M-ABCA7

APP processing.[9,11,12,15,16,19,55,56] Human ABCA7 can promote phospholipid and, to a certain degree, cholesterol efflux to apolipoproteins in vitro.[7,9,11,56] More recently, an in vitro model of the blood-brain barrier was used to demonstrate an effect of ABCA7 on regulation of cholesterol and Aβ efflux.[57] Consistent with these findings, we find that homozygosity for the V1613M variant in mice influences brain lipids in a relatively minor manner compared to WT control mice, and that ABCA7, along with the V1613M variant, did not strongly affect cholesterol efflux in neuronal cells in vitro. However, despite this, circulating cholesterol levels are increased in *Abca7*^{V1613M} mice suggesting that other cell types in the body may be having greater effects on cholesterol metabolism or transport. Further, when combined with an amyloidogenic insult produced by the 5xFAD transgene array, the V1613M variant produces an increase in a wide range of brain lipids in addition to increasing circulating cholesterol and triglycerides. Most significantly, we demonstrate that the V1613M variant has a profound effect on APP processing and Aβ plaque deposition in hemizygous 5xFAD mice.

Loss of ABCA7 function has been associated with increased amyloid deposition in humans via neuroimaging studies.[58,59] Aβ is cleaved from its precursor, APP, via the amylogenic pathway which is mediated first by β-secretase (BACE1), producing soluble APPβ (sAPPβ) and C99 fragments, followed by γ-secretase to release Aβ and AICD. Studies using distinct human APP transgenic mouse models show that KO of *Abca7* in both TgCRND8 and APP/PS1 mice results in increased Aβ pathology as well as increased levels of sAPPβ and soluble Aβ.[12,19] In contrast, here we find that the *Abca7*^{V1613M} variant robustly decreases plaque load and Aβ generation in 5xFAD mice, across multiple timepoints, suggesting that this variant is not a loss of function, but rather promotes ABCA7 functions by increasing normal functions (ie, hypermorphic) or developing new functions (ie, neomorphic), or a combination of both. We also observed a reduction in downstream reactions to plaques, including in astrocyte reactivity, accumulation of dystrophic neurites and presence of NfL in the periphery, but no differences in synapse loss compared to 5xFAD mice. Whether these reductions are a consequence of the reduced plaque load in 5xFAD/*Abca7*^{V1613M} mice or due to an ABCA7-driven mechanism remains to be determined.

Our study demonstrates that the *Abca7*^{V1613M} variant robustly decreases steady-state levels of both C99 and C83, along with a decrease in full-length APP in the brain of hemizygous 5xFAD mice. Overexpression of ABCA7 can produce a similar phenotype in both APPwt and APPswe overexpressing CHO cells, also resulting in decreases in SAPPβ and Aβ and localization of APP in perinuclear and other subcellular structures.[56] The reduction in both C99 and C83 is not consistent with inhibition or promotion of either the α- or β-secretase pathways as they compete for substrate (APP), but instead suggests that APP is located in a manner that reduces its availability to either pathway equally. To assess whether ABCA7 also influenced the subcellular localization of APP, and therefore its availability to be processed, we overexpressed WT or V1613M mouse ABCA7 in N2a cells and stained for APP and markers of the endo-lysosomal pathway. The increase in intracellular APP puncta in N2a cells overexpressing the ABCA7 V1613M variant compared to WT ABCA7 and their colocalization with LAMP1 and RAB7A structures is consistent with a model of increased accumulation of APP in endo-lysosomal structures, which could result in increased degradation accounting for the equal reductions in both C99 and C83, as well as full-length APP.

In addition to effects on Aβ generation and plaque pathology, KO of ABCA7 can modulate microglia and macrophage function.[15–17] Microglia are key mediators of AD pathology and by constantly sensing their surroundings, they can facilitate responses to different stimuli.[60–62] To assess whether the V1613M variant affects microglial function we assessed microglial response to acute stimulation via LPS injection and chronic stimulation, by their reaction to plaques. The results indicate that homozygosity for the V1613M variant extends the response to LPS stimulation, characterized by prolonged increase in classical proinflammatory genes such as *C1qa*, *C1qb*, *C1qc*, *C1ra*, and *Hcar2*. One possible explanation for this prolonged response in *Abca7*^{V1613M} mice could be the downregulation of *Dok3* in *Abca7*^{V1613M} homozygous mice compared to WT mice under homeostatic conditions (Figure 1B). *Dok3* is a negative regulator of LPS-mediated inflammation and reduced expression of *Dok3* results in increased LPS signaling in macrophages.[28] To explore if *Abca7*^{V1613M} was modulating the phagocytic abilities of microglia we incubated primary microglia from WT and *Abca7*^{V1613M} mice with beads, which represent dead/dying cells, and Aβ1-42 peptide. Microglia from homozygous *Abca7*^{V1613M} have increased phagocytic capacity for both beads and Aβ1-42. In contrast to our findings in vitro and in response to acute stimulation, we did not find striking differences in microglial responses to chronic stimulation (Aβ plaques) in 5xFAD mice with the *Abca7*^{V1613M} variant. Microglial numbers and associated inflammatory response reflected

FIGURE 6 *Abca7*^{V1613M} variant reduces amyloid beta (Aβ) production and processing in vivo and alters amyloid precursor protein (APP) trafficking in vitro. (A-P) Quantification of Aβ40 and Aβ42 in detergent insoluble and soluble fractions in 5xFAD and 5XFAD/*Abca7*^{V1613M} hippocampus and cortex in (A-H) 4 month-old and (I-P) 12-month-old mice. In 4-month-old mice, both Aβ40 and Aβ42 are reduced in all samples. At 12-months-old, soluble Aβ40 and Aβ42 are reduced in subiculum and insoluble Aβ40 is reduced in cortex, with both soluble and insoluble Aβ40 and Aβ42 trending lower in other samples from 5xFAD/*Abca7*^{V1613M} animals compared to 5xFAD mice. (Q) Western blot of soluble cortical protein from representative female 5xFAD and 5XFAD/*Abca7*^{V1613M} mice at 4 months for full-length APP (FL-APP), APP C-terminal fragments (C99 and C83), BACE-1, ADAM-10, PSEN1, and C-terminal PSEN1 fragment. (R) Quantification of FL-APP, C99 and C83, BACE-1, ADAM-10, and PSEN1 normalized to total protein stain (TPS) as a percentage of 5xFAD signal intensity. (S) Quantification of intracellular APP+ puncta in transfected N2a cells. (T-W) Representative confocal images showing 22C11 (APP) and LAMP1 staining in (T) nontransfected control, (U) EGFP-only (empty vector) control, (V) Wildtype (WT)-ABCA7 overexpressing, and (W) V1613M-ABCA7 overexpressing N2a cells. Scale bar = 2 microns. $N = 4$ to 6 per sex/genotype/age (A-R); $N = 26$ to 36 cells per group (S). Data are represented as mean ± SEM. Statistics (A-P) by unpaired Student *t*-test, (R) by individual unpaired Student *t*-test of each target protein, (S) by one-way analysis of variance. $^{*}p \leq 0.05$, $^{**}p \leq 0.01$, $^{***}p \leq 0.001$, $^{****}p \leq 0.0001$.

reduced Aβ plaque numbers in 5xFAD/*Abca7*^{V1613M} mice. Thus, despite high expression of ABCA7 in microglia, this variant does not appear to grossly alter microglial function, in disease context, but rather its effect may be more prominent in neurons on Aβ generation and deposition in the aging brain rather than the reaction to the plaques driving damage and clinical symptoms. These different responses to different stimuli, acute versus chronic, may be due to the distinct recognition and signaling mechanisms of microglial activation associated with these different insults, further highlighting the complex nature of microglial function in health and disease.

This study is the first to explore functions of the V1599M (humans)/V1613M (mice) AD-associated ABCA7 variant. 5xFAD/*Abca7*^{V1613M} mice display persistent reductions in Aβ and plaque numbers. This reduction is mirrored by reduced inflammation, associated microgliosis, astrogliosis, and pathology-induced damage. 5xFAD/*Abca7*^{V1613M} mice also exhibit altered APP processing. Our data suggest that the *Abca7*^{V1613M} variant is not a loss of function mutation, counter to the original predictions, but rather may act as a neomorph. These data raise the interesting possibility that the rs117187003 *ABCA7* V1599M variant might be protective and potentially larger cohorts of individuals harboring *ABCA7*^{V1599M} are required to elucidate this.

ACKNOWLEDGMENTS

The authors thank Dr. Masashi Kitazawa (UC Irvine) for generously providing mouse N2a neuroblastoma cells and the UC Davis West Coast Metabolomics Center for bulk lipidomics analyses. This study was made possible in part through access to the Optical Biology Core Facility of the Developmental Biology Center, and the UCI Transgenic Mouse Facility (TMF), shared resources supported by the Cancer Center Support Grant (CA-62203) and Center for Complex Biological Systems Support Grant (GM-076516) at the University of California, Irvine.

CONFLICT OF INTEREST STATEMENT

KNG is a member of the advisory board of Ashvattha Therapeutics. Author disclosures are available in the supporting information. This study was supported by the Model Organism Development and Evaluation for Late-onset Alzheimer's Disease (MODEL-AD) consortium funded by the National Institute on Aging (U54 AG054349).

DATA AVAILABILITY STATEMENT

Protocols, data, and results are available via the AD Knowledge Portal (https://adknowledgeportal.synapse.org). The AD Knowledge Portal is a platform for accessing data, analyses, and tools generated by the Accelerating Medicines Partnership (AMP-AD) Target Discovery Program and other National Institute on Aging (NIA)-supported programs to enable open-science practices and accelerate translational learning. The data, analyses, and tools are shared early in the research cycle without a publication embargo on secondary use. Data are available for general research use according to the following requirements for data access and data attribution (https://adknowledgeportal.org/DataAccess/Instructions). Data can be accessed in an interactive matter at UCI Mouse Mind Explorer (admodelexplorer.org).

The *Abca7*^{V1613M} model is available from The Jackson Laboratory (Stock #035316) without restrictions on its use by both academic and commercial users. The content is solely the responsibility of the authors and does not necessarily represent the official view of the National Institutes of Health.

CONSENT STATEMENT

No human subjects were used for the present study. Therefore, consent was not necessary.

REFERENCES

1. Knopman DS, Amieva H, Petersen RC, et al. Alzheimer disease. *Nat Rev Dis Primers*. 2021;7(1):33.
2. Lambert JC, Ibrahim-Verbaas CA, Harold D, et al. Meta-analysis of 74,046 individuals identifies 11 new susceptibility loci for Alzheimer's disease. *Nat Genet*. 2013;45(12):1452-1458.
3. Reitz C, Jun G, Naj A, et al. Variants in the ATP-binding cassette transporter (ABCA7), apolipoprotein E ε4,and the risk of late-onset Alzheimer disease in African Americans. *JAMA*. 2013;309(14):1483-1492.
4. Vardarajan BN, Ghani M, Kahn A, et al. Rare coding mutations identified by sequencing of Alzheimer disease genome-wide association studies loci. *Ann Neurol*. 2015;78(3):487-498.
5. Hollingworth P, Harold D, Sims R, et al. Common variants at ABCA7, MS4A6A/MS4A4E, EPHA1, CD33 and CD2AP are associated with Alzheimer's disease. *Nat Genet*. 2011;43(5):429-435.
6. Kim WS, Weickert CS, Garner B. Role of ATP-binding cassette transporters in brain lipid transport and neurological disease. *J Neurochem*. 2008;104(5):1145-1166.
7. Picataggi A, Rodrigues A, Cromley DA, et al. Specificity of ABCA7-mediated cell lipid efflux. *Biochim Biophys Acta Mol Cell Biol Lipids*. 2022;1867(7):159157.
8. Wiener JP, Desire S, Garliyev V, Lyssenko Iii N, Praticò D, Lyssenko NN. Down-regulation of ABCA7 in human microglia, astrocyte and THP-1 cell lines by cholesterol depletion, IL-1β and TNFα, or PMA. *Cells*. 2023;12(17).
9. Wang N, Lan D, Gerbod-Giannone M, et al. ATP-binding cassette transporter A7 (ABCA7) binds apolipoprotein A-I and mediates cellular phospholipid but not cholesterol efflux. *J Biol Chem*. 2003;278(44):42906-42912.
10. Abe-Dohmae S, Yokoyama S. ABCA7 links sterol metabolism to the host defense system: molecular background for potential management measure of Alzheimer's disease. *Gene*. 2021;768:145316.
11. Abe-Dohmae S, Ikeda Y, Matsuo M, et al. Human ABCA7 supports apolipoprotein-mediated release of cellular cholesterol and phospholipid to generate high density lipoprotein. *J Biol Chem*. 2004;279(1):604-611.
12. Sakae N, Liu CC, Shinohara M, et al. ABCA7 deficiency accelerates amyloid-beta generation and Alzheimer's neuronal pathology. *J Neurosci*. 2016;36(13):3848-3859.
13. Nowyhed HN, Chandra S, Kiosses W, et al. ATP binding cassette transporter ABCA7 regulates NKT cell development and function by controlling CD1d expression and lipid raft content. *Sci Rep*. 2017;7:40273.
14. Fu Y, He Y, Phan K, et al. Sex-specific lipid dysregulation in the Abca7 knockout mouse brain. *Brain Commun*. 2022;4(3):fcac120.
15. Jehle AW, Gardai SJ, Li S, et al. ATP-binding cassette transporter A7 enhances phagocytosis of apoptotic cells and associated ERK signaling in macrophages. *J Cell Biol*. 2006;174(4):547-556.
16. Kim WS, Li H, Ruberu K, et al. Deletion of Abca7 increases cerebral amyloid-β accumulation in the J20 mouse model of Alzheimer's disease. *J Neurosci*. 2013;33(10):4387-4394.

17. Aikawa T, Ren Y, Yamazaki Y, et al. ABCA7 haplodeficiency disturbs microglial immune responses in the mouse brain. *Proc Natl Acad Sci U S A*. 2019;116(47):23790-23796.
18. Fu Y, Hsiao JH, Paxinos G, Halliday GM, Kim WS. ABCA7 mediates phagocytic clearance of amyloid-beta in the brain. *J Alzheimers Dis*. 2016;54(2):569-584.
19. Satoh K, Abe-Dohmae S, Yokoyama S, St George-Hyslop P, Fraser PE. ATP-binding cassette transporter A7 (ABCA7) loss of function alters Alzheimer amyloid processing. *J Biol Chem*. 2015;290(40):24152-24165.
20. Bossaerts L, Hendrickx Van de Craen E, Cacace R, Asselbergh B, Van Broeckhoven C. Rare missense mutations in ABCA7 might increase Alzheimer's disease risk by plasma membrane exclusion. *Acta Neuropathol Commun*. 2022;10(1):43.
21. Sassi C, Nalls MA, Ridge PG, et al. ABCA7 p.G215S as potential protective factor for Alzheimer's disease. *Neurobiol Aging*. 2016;46:235.e1-9.
22. Rezaie N, Reese F, Mortazavi A. PyWGCNA: a Python package for weighted gene co-expression network analysis. *bioRxiv*. 2022. 2022.08.22.504852.
23. Carrillo-Jimenez A, Puigdellívol M, Vilalta A, et al. Effective knockdown of gene expression in primary microglia with siRNA and magnetic nanoparticles without cell death or inflammation. *Front Cell Neurosci*. 2018;12:313.
24. Cajka T, Smilowitz JT, Fiehn O. Validating quantitative untargeted lipidomics across nine liquid chromatography-high-resolution mass spectrometry platforms. *Anal Chem*. 2017;89(22):12360-12368.
25. Forner S, Kawauchi S, Balderrama-Gutierrez G, et al. Systematic phenotyping and characterization of the 5xFAD mouse model of Alzheimer's disease. *Sci Data*. 2021;8(1):270.
26. Javonillo DI, Tran KM, Phan J, et al. Systematic phenotyping and characterization of the 3xTg-AD mouse model of Alzheimer's Disease. *Front Neurosci*. 2021;15:785276.
27. Tran KM, Kawauchi S, Kramár EA, et al. A Trem2(R47H) mouse model without cryptic splicing drives age- and disease-dependent tissue damage and synaptic loss in response to plaques. *Mol Neurodegener*. 2023;18(1):12.
28. Peng Q, O'Loughlin JL, Humphrey MB. DOK3 negatively regulates LPS responses and endotoxin tolerance. *PLoS One*. 2012;7(6):e39967.
29. Ikeda Y, Abe-Dohmae S, Munehira Y, et al. Posttranscriptional regulation of human ABCA7 and its function for the apoA-I-dependent lipid release. *Biochem Biophys Res Commun*. 2003;311(2):313-318.
30. Truesdale KP, Stevens J, Cai J. The effect of weight history on glucose and lipids: the Atherosclerosis Risk in Communities Study. *Am J Epidemiol*. 2005;161(12):1133-1143.
31. Serrano-Pozo A, Frosch MP, Masliah E, Hyman BT. Neuropathological alterations in Alzheimer disease. *Cold Spring Harb Perspect Med*. 2011;1(1):a006189.
32. Spires-Jones TL, Hyman BT. The intersection of amyloid beta and tau at synapses in Alzheimer's disease. *Neuron*. 2014;82(4):756-771.
33. Kang MS, Aliaga AA, Shin M, et al. Amyloid-beta modulates the association between neurofilament light chain and brain atrophy in Alzheimer's disease. *Mol Psychiatry*. 2021;26(10):5989-6001.
34. Keren-Shaul H, Spinrad A, Weiner A, et al. A unique microglia type associated with restricting development of Alzheimer's disease. *Cell*. 2017;169(7):1276-1290. e17.
35. Naj AC, Jun G, Beecham GW, et al. Common variants at MS4A4/MS4A6E, CD2AP, CD33 and EPHA1 are associated with late-onset Alzheimer's disease. *Nat Genet*. 2011;43(5):436-441.
36. Cuyvers E, De Roeck A, Van den Bossche T, et al. Mutations in ABCA7 in a Belgian cohort of Alzheimer's disease patients: a targeted resequencing study. *Lancet Neurol*. 2015;14(8):814-822.
37. Kunkle BW, Carney RM, Kohli MA, et al. Targeted sequencing of ABCA7 identifies splicing, stop-gain and intronic risk variants for Alzheimer disease. *Neurosci Letters*. 2017;649:124-129.
38. Cukier HN, Kunkle BW, Vardarajan BN, et al. ABCA7 frameshift deletion associated with Alzheimer disease in African Americans. *Neurol Genet*. 2016;2(3):e79.
39. Steinberg S, Stefansson H, Jonsson T, et al. Loss-of-function variants in ABCA7 confer risk of Alzheimer's disease. *Nat Genet*. 2015;47(5):445-447.
40. Allen M, Lincoln SJ, Corda M, et al. ABCA7 loss-of-function variants, expression, and neurologic disease risk. *Neurol Genet*. 2017;3(1):e126.
41. Bellenguez C, Charbonnier C, Grenier-Boley B, et al. Contribution to Alzheimer's disease risk of rare variants in TREM2, SORL1, and ABCA7 in 1779 cases and 1273 controls. *Neurobiol Aging*. 2017;59:220. e1- e9.
42. De Roeck A, Van den Bossche T, van der Zee J, et al. Deleterious ABCA7 mutations and transcript rescue mechanisms in early onset Alzheimer's disease. *Acta Neuropathol*. 2017;134(3):475-487.
43. Lyssenko NN, Shi X, Praticò D. The Alzheimer's disease GWAS risk alleles in the ABCA7 promoter and 5' region reduce ABCA7 expression. *Acta Neuropathol*. 2022;144(3):585-587.
44. Lyssenko NN, Praticò D. ABCA7 and the altered lipidostasis hypothesis of Alzheimer's disease. *Alzheimers Dement*. 2021;17(2):164-174.
45. Holstege H, Hulsman M, Charbonnier C, et al. Exome sequencing identifies rare damaging variants in ATP8B4 and ABCA1 as risk factors for Alzheimer's disease. *Nat Genet*. 2022;54(12):1786-1794.
46. N'Songo A, Carrasquillo MM, Wang X, et al. African American exome sequencing identifies potential risk variants at Alzheimer disease loci. *Neurol Genet*. 2017;3(2):e141.
47. Nygaard HB, Erson-Omay EZ, Wu X, et al. Whole-exome sequencing of an exceptional longevity cohort. *J Gerontol A Biol Sci Med Sci*. 2019;74(9):1386-1390.
48. Lee WP, Choi SH, Shea MG, et al. Association of common and rare variants with Alzheimer's Disease in over 13,000 diverse individuals with whole-genome sequencing from the Alzheimer's disease sequencing project. *medRxiv*. 2023.
49. Zhang Y, Chen K, Sloan SA, et al. An RNA-sequencing transcriptome and splicing database of glia, neurons, and vascular cells of the cerebral cortex. *J Neurosci*. 2014;34(36):11929-11947.
50. De Roeck A, Van Broeckhoven C, Sleegers K. The role of ABCA7 in Alzheimer's disease: evidence from genomics, transcriptomics and methylomics. *Acta Neuropathol*. 2019;138(2):201-220.
51. Mathys H, Davila-Velderrain J, Peng Z, et al. Single-cell transcriptomic analysis of Alzheimer's disease. *Nature*. 2019;570(7761):332-337.
52. Morabito S, Miyoshi E, Michael N, et al. Single-nucleus chromatin accessibility and transcriptomic characterization of Alzheimer's disease. *Nat Genet*. 2021;53(8):1143-1155.
53. Morabito S, Miyoshi E, Michael N, Swarup V. Integrative genomics approach identifies conserved transcriptomic networks in Alzheimer's disease. *Hum Mol Genet*. 2020;29(17):2899-2919.
54. Leng K, Li E, Eser R, et al. Molecular characterization of selectively vulnerable neurons in Alzheimer's disease. *Nat Neurosci*. 2021;24(2):276-287.
55. Kim WS, Fitzgerald ML, Kang K, et al. Abca7 null mice retain normal macrophage phosphatidylcholine and cholesterol efflux activity despite alterations in adipose mass and serum cholesterol levels. *J Biol Chem*. 2005;280(5):3989-3995.
56. Chan SL, Kim WS, Kwok JB, et al. ATP-binding cassette transporter A7 regulates processing of amyloid precursor protein in vitro. *J Neurochem*. 2008;106(2):793-804.
57. Lamartinière Y, Boucau MC, Dehouck L, et al. ABCA7 downregulation modifies cellular cholesterol homeostasis and decreases amyloid-β peptide efflux in an in vitro model of the blood-brain barrier. *J Alzheimers Dis*. 2018;64(4):1195-1211.

58. Hughes TM, Lopez OL, Evans RW, et al. Markers of cholesterol transport are associated with amyloid deposition in the brain. *Neurobiol Aging*. 2014;35(4):802-807.
59. Apostolova LG, Risacher SL, Duran T, et al. Associations of the Top 20 Alzheimer disease risk variants with brain amyloidosis. *JAMA Neurol*. 2018;75(3):328-341.
60. Wolf SA, Boddeke HW. Kettenmann H. microglia in physiology and disease. *Annu Rev Physiol*. 2017;79:619-643.
61. Vilalta A, Brown GC. Neurophagy, the phagocytosis of live neurons and synapses by glia, contributes to brain development and disease. *Febs j*. 2018;285(19):3566-3575.
62. Galloway DA, Phillips AEM, Owen DRJ, Moore CS. Phagocytosis in the Brain: homeostasis and Disease. *Front Immunol*. 2019;10:790.

SUPPORTING INFORMATION

Additional supporting information can be found online in the Supporting Information section at the end of this article.

How to cite this article: Butler CA, Mendoza Arvilla A, Milinkeviciute G, et al. The *Abca7*^{V1613M} variant reduces Aβ generation, plaque load, and neuronal damage. *Alzheimer's Dement*. 2024;20:4914–4934.
https://doi.org/10.1002/alz.13783